A novel brain tumour model in zebrafish reveals the role of YAP activation in MAPK- and PI3K-induced malignant growth

DMM Advance Online Articles. Posted 24 November 2016 as doi: 10.1242/dmm.026500
Access the most recent version at http://dmm.biologists.org/lookup/doi/10.1242/dmm.026500

A novel brain tumour model in zebrafish reveals the role of YAP activation in MAPK/PI3K induced malignant growth.

Marie Mayrhofer[1], Victor Gourain[1], Markus Reischl[2], Pierre Affaticati[3], Arnim Jenett[3], Jean-Stephane Joly[3], Matteo Benelli[6], Francesca Demichelis[6], Pietro Luigi Poliani[5], Dirk Sieger[4] and Marina Mione[1,6*]

[1]Institute for Toxicology and Genetics, [2]Institute for Applied Informatics at Karlsruhe Institute of Technology, Hermann von Helmholtz Platz 1, Eggenstein-Leopoldshafen, 76344, Germany; [3]Tefor Core Facility, Paris-Saclay Institute of Neuroscience, CNRS, Université Paris-Saclay, 91190 Gif-sur-Ivette, France; [4]Centre for Neuroregeneration, The University of Edinburgh, The Chancellor's Building, 49 Little France Crescent, Edinburgh EH16 4SB, United Kingdom; [5]Department of Molecular and Translational Medicine, Pathology Unit, University of Brescia School of Medicine, Spedali Civili Brescia, 25123, Brescia, Italy; [6]Centre for Integrative Biology, University of Trento, Via Sommarive 9, 38123 Trento, Italy.

*Corresponding Author: mariacaterina.mione@unitn.it

keywords: glioma, YAP, RAS, zebrafish

Summary statement

A new brain tumour model in zebrafish allows simultaneous analysis of malignant tumours and heterotopias, suggesting that both lesions originate from similar events, with Yap1 as a driving force in tumour development.

Abstract

Somatic mutations activating MAPK/PI3K signalling play a pivotal role in both tumours and brain developmental disorders. We developed a zebrafish model of brain tumour based on somatic expression of oncogenes that activate MAPK/PI3K signalling in neural progenitor cells. $HRAS^{V12}$ was the most effective in inducing both heterotopia and invasive tumours. Tumours, but not heterotopias, require persistent activation of phospho-(p)ERK and express a gene signature similar to the mesenchymal glioblastoma subtype, with a strong YAP component. Application of a 8-gene signature to human brain tumours establishes that YAP activation distinguishes between mesenchymal glioblastoma and low grade glioma in a wide TCGA sample set including gliomas and glioblastomas (GBMs). This suggests that the activation of YAP may be an important event in brain tumour development, promoting malignant versus benign brain lesions. Indeed, co-expression of dominant active YAP (YAP^{S5A}) and $HRAS^{V12}$ abolishes the development of heterotopias and leads to the sole development of aggressive tumours. Thus, we have developed a model proving that neurodevelopmental disorders and brain tumours may originate from the same somatic mutations activating oncogenes and established that YAP activation is a hallmark of malignant brain tumours.

Introduction

Disorders of brain growth are known to cause a wide range of physiological and pathological symptoms such as intractable epilepsy, intellectual disability, autism, cognitive and motor impairment (Aronica and Crino, 2014, Courchesne et al., 2001, Hevner, 2015). Their causes are diverse and comprise: (i) focal lesions characterised by abnormal location of otherwise normally differentiated neural cells (Thom et al., 2004), (ii) "tuberous" formation and similar disorders with abnormally large neurons and/or other cell types (Blumcke et al., 2011, Crino, 2013) and (iii) brain overgrowth syndromes leading to diffuse megalencephaly or malformations (Winden et al., 2015), which are mostly limited to developmental stages. By contrast, paediatric and adult primary malignant brain tumours are characterised by the sustained proliferation of poorly differentiated or abnormal neural cells. Both types of diseases (brain growth disorders and tumours) may initially appear with similar symptoms and share a similar origin from somatic mutations (Blumcke et al., 2011), which is confirmed by co-occurrence of both disorders in the same patients (Johansson et al., 2015). For example, coexistence of developmental disorders and brain tumours is commonly observed in neurofibromatosis type 1 (Reuss and von Deimling, 2009) (NF1), a genetic disorder that afflicts 1 in about 3000 newborns (Evans et al., 2010). NF1 is caused by loss-of-function mutations in the tumour suppressor gene NF1, which encodes neurofibromin 1, a negative regulator of the proto-oncogene RAS (Ballester et al., 1990, Cichowski and Jacks, 2001) and in 50 % of cases occurs as the result of *de novo* somatic mutations. 5-10 % of patients with tuberous sclerosis (caused by mutations in TSC1 or TSC2, OMIN 191100) develop slowly growing subependymal giant cell astrocytomas (Grajkowska et al., 2010) and in 50 % of patients with focal cortical dysplasia type 3b cortical disorganisation masks slowly-developing brain tumours (Blumcke et al., 2011, Palmini et al., 2013, Santos et al., 2014).
However, for most developmental disorders of the brain it is currently unknown whether focal or diffuse growth disorders may progress to tumours due to additional mutations or epigenetic events. Although the molecular pathogenesis of these disorders are currently unknown, for most of them genetic studies show that activation of MAPK/PI3K or mTOR signals due to *de novo* somatic mutations or inherited germline mutations may be causative (for review see (Aronica and Crino, 2014, Barkovich et al., 2012, Dyment et al., 2013, Hevner, 2015). These pathways are also altered in gliomas, as leading mutations in high grade gliomas include EGFR amplification (in 27-36 % of cases, (Ohgaki and Kleihues, 2007) or mutations (18-31 % of cases, (Liu et al., 2005), deletion of PTEN, the inhibitor of AKT and mTOR (15-40 %

of cases, (Tohma et al., 1998) and inactivation of NF1, a RAS inhibitor (18 % of cases, TCGA (Network, 2008). While only few gliomas contain mutation in RAS itself, the leading mutations reported above affect its activity in nearly all glioma cases (Jones et al., 2012, Patil et al., 2013). On the other hand, activation of Ras/Raf is the molecular hallmark of pilocytic astrocytoma (a grade I astrocytoma, which rarely progresses to higher grade (Jones et al., 2008).

While separate models for developmental disorders or brain tumour diseases exist (Fomchenko and Holland, 2006, Stylli et al., 2015, Wong and Roper, 2015), models of progressive brain developmental disorders with spontaneous cancerous development are lacking. Such models may allow the study of the molecular events leading to tumour development starting from benign developmental lesions, the identification of the mechanisms of tumour suppression in those cases that do not progress and the development of preventive therapies. These models may also be instrumental in understanding the progression from benign to malignant brain tumours, such as glioblastoma (GBM), which occurs in ~50 % of patients diagnosed with grade II and grade III gliomas (Chaichana et al., 2010, Ho et al., 2016, Louis et al., 2007).

Glioma progression has been linked to a number of pathway alterations including EGFR/MAPK/PTEN and p53 signalling (Ohgaki and Kleihues, 2009). Additionally, the transcriptional co-activators YAP/TAZ of the Salvador-Warts-Hippo pathway have been linked to glioma progression and poor patient survival (Bhat et al., 2011, Orr et al., 2011). An increase of YAP/TAZ activity has been documented in high grade gliomas, while they are significantly less active in low grade gliomas (Orr et al., 2011). In cell culture experiments YAP/TAZ promote glioma cell proliferation, invasion and resistance to apoptosis (Bhat et al., 2011, Orr et al., 2011). However, their impact on the progression of low grade gliomas is still poorly documented.

In this study we have generated a zebrafish model of focal brain growth disorders through the expression of different oncogenes in neural cells during development. These focal growths are of two types: either they result in dislocation of neural cells (or duplication of neural structures) without further growth, malformations defined as “heterotopias” or in malignant brain tumours. Thus, this model provides novel insights into the relation between benign lesions and aggressive tumours as it shows: i) that RAS/MAPK signalling can induce both heterotopia (non-cancerous benign lesions) and aggressive brain tumours, ii) that aggressive tumours have a mesenchymal GBM signature, iii) that activation of YAP signalling distinguishes aggressive tumours from heterotopia and iv) that forcing the activation of YAP

signalling at earlier stages promotes aggressive tumours at the expenses of heterotopia. These data indicate a central role for YAP activation in the progression of benign growth disorders to aggressive tumours and suggest the possibility of preventing it by specific inhibitors.

Results

Activation of the EGFR/RAS/ERK/AKT pathway through the zic4 enhancer induces brain tumour development.

To generate a brain tumour model, we used the Gal4-UAS system to induce expression of different oncogenes under the UAS promoter in the driver line Et(zic4:GAL4TA4,UAS:mCherry)$_{hmz5}$ (Distel et al., 2009), further on referred to as zic:Gal4. This line expresses the codon-optimised version of the transcription factor Gal4 under control of the zic4 enhancer in the proliferating domains of the developing central nervous system (Fig. S1A-C') which is visualised through mCherry expression. Zic:Gal4 is also expressed in the adult brains (Fig. S1C, C') as documented previously for the endogenous zic4 gene (Aruga, 2004, Grinberg and Millen, 2005). We used different UAS-driven oncogenes, some activating the EGFR/RAS/ERK/AKT pathway, already reported to generate neoplasia in the zebrafish brain (GFP-KRAS^{V12} (Ju et al., 2015), AKT (Jung et al., 2013), others known as oncogenic in human brain (GFP-EGFR $_{\text{transcript variant III (vIII)}}$ (Liu et al., 2005), also represented by Xmrk, the oncogenic version of the EGFR in Xiphoporus, and BRAF^{E600} (Penman et al., 2015) (see Table S1 for list and full names of constructs). All these oncogenes induced tumour formation (Fig. S2A-D, Table S2) and all but AKT induced ERK phosphorylation (Fig. S2E), with GFP-HRAS^{V12} exhibiting the strongest effect.

To analyse the effect of activated RAS on tumour development, we generated both germline and somatic UAS:GFP-HRAS^{V12} expressing animals. To induce germline UAS:GFP-HRAS^{V12} expression (shortened in zic:RAS$_{germline}$, Fig. 1A), we crossed the line zic:Gal4 to the line *tg(UAS:eGFP-HRASv12)$_{io006}$* (Santoriello et al., 2010) (further on referred to as UAS:RAS). To induce somatic GFP-HRAS^{V12} expression (zic:RAS$_{somatic}$, Fig. 1B), embryos of the line zic:Gal4 were injected at 1-cell stage with the plasmid UAS:GFP-HRAS^{V12}. F0 embryos expressing the transgene were identified by GFP expression and used for further analysis.

Both approaches induced early but different effects. The germline approach affected all zic4^{+} cells in the brain (Fig. 1C-D') and already at 3 dpf led to a constant increase in brain size of 2.3 times (Fig. 1E) which was accompanied by a similar increase in the number of proliferating cells (91.6 ± 11.0, n=5, in zic:RAS versus 34.1 ± 6.2, n=5, in zic:Gal4 larvae) as determined through BrdU staining (2.7 fold, Fig. 1F). The somatic approach instead lead to random oncogene expression in the zic4^{+} cell population affecting single cells in different

number and localisation (Fig. 1G-G"). Hence, it allowed for detailed time lapse analysis of the affected cells, which revealed their clonal expansion in larvae (Fig. 1H-H'"). Even though both approaches lead to tumour formation, the difference between them is mostly reflected in their survival with the germline approach enabling only 4 % ± 1.2 % to survive the first month while the somatic approach allows 36.9 % ± 5.9 % to survive (Fig. 1I).

Therefore, germline expression of UAS:GFP-HRAS^{V12} in the brain of developing zebrafish induces highly reproducible effects enabling the possible application of this model in screening approaches. The somatic expression of UAS:GFP-HRAS^{V12} instead is ideal for single cell analysis as well as investigation of mechanisms of clonal expansion and oncogenesis up to later stages.

Expression of the oncogene GFP-HRAS^{V12} induces brain tumours and/or heterotopia

Next, brains of juvenile and adult fish (1-14 months) were resected and whole brains imaged for bright field and fluorescence. The observations unravelled the development of abnormal brain structures which could be grouped into malformations with and (mostly) without GFP-expression; Fig. 2A-C). Both types of malformations occurred with the germline and with the somatic approach and were often found in the same brain (Table S2) but never in control injected fish (data not shown). Specifically, the analysis of 134 brains of zic:RAS$_{somatic}$ fish revealed that 81.2 % of the brains developed GFP$^+$ malformations, appearing most frequently in the telencephalon (62.4 %), in the IVth ventricle (33.1 %) and in the diencephalon (30.1 %). However, 50.4 % of the fish developed malformations, which were mostly GFP-negative (i.e. with only a few GFP$^+$ cells, which for brevity we call GFP$^-$); both types of malformations could be present in the same brain (Fig. 2D). 3D reconstruction allowed analysis of the infiltrative nature of GFP-expressing lesions (Fig. 2E-F) while GFP$^-$ malformations appeared as sharply circumscribed structures without penetration into deeper layers (Fig. 2G, white arrow). Further, the 3D reconstruction allowed to predict that several clones contributed to the large GFP$^+$ malformations, which we interpreted as cancerousgrowths based on the analysis reported in the next paragraphs (Fig. 2H).

Specific immunohistochemical signatures establish that GFP-HRAS^{V12} positive lesions are tumours and show persistent activation of MAPK/ERK signalling.

The relation between developmental brain lesions and glioma has been the focus of a number of recent reports (Hevner, 2015, Marin-Valencia et al., 2014, Reuss and von Deimling, 2009), raising the question as to whether developmental brain growth disorders (including focal dysplasia and heterotopia (Aronica and Crino, 2014, Hevner, 2015) may be the result of halted oncogenic events taking place during development and/or provide a substrate for brain tumour development. In our model, the same oncogenes lead to two types of lesions, one resembling cancer and the other resembling heterotopia, thus providing an opportunity to study possible co-factors, that may induce benign developmental lesions instead of tumours. The different nature of these lesions was assessed through H&E staining by an expert neuropathologist (PLP), who also recognised peculiar features associated to tumours developing in the different areas of the brain, spanning from embryonal to more differentiated histopathological features, suggesting that these zebrafish brain tumours may resemble different histological subtypes of Central Nervous System tumours (Louis et al., 2016). To further clarify these differences and understand why in some instances the oncogene HRAS^{V12} expressed in brain progenitor cells induced tumour development and in other cases produced only heterotopias, we investigated the expression of different markers by immunofluorescence: BrdU uptake for proliferation, GFAP for glial cells, S100β for progenitor cells, HU-C for neurons and p-ERK for MAPK activity.

The pattern of staining for these markers was disrupted in tumours and in heterotopias in different ways. Specifically, in the telencephalon, tumours (present in 62.4 % of the injected fish, "T" in Fig. 2B) appeared as diffusely infiltrating malignant masses (Fig. 3A-C) showing strong cellular heterogeneity (Fig. 3D) and a high proliferation index (Fig. 3E-F). Besides proliferation, we assessed p-ERK levels, number of HU-C+ and S100β+ cells and GFAP staining. A summary of the stainings present in GFP+ tumours arising in different brain regions is shown in Fig. 3 and Fig. S3.

GFP negative (-) heterotopias (present in 50.4 % of the injected fish, Fig. 2C) were defined as ectopically localised groups of cells, lacking or with only a mild atypia and basically reproducing normal neural cell types but in the wrong location and/or in a larger number, reminiscent of a lack of maturation or migration and/or prolonged proliferation. They were easily visualised in the optic tectum (Fig. 3K-T), thanks to its layered structure, but also occurred in the telencephalon (Fig. S4A-A') and in the cerebellum (Fig. S4B-B'). P-ERK

staining in the heterotopias was absent (Fig. 3Q), while HU-C, GFAP (Fig. 3R-S) and S100β (Fig. 3T) were similar to those in the adjacent periventricular grey zone, from which the optic tectum heterotopias seem to originate. This suggested that normal developmental processes in these lesions were not subverted like in tumours, but just delayed or mis-localised. Most notably, UAS:GFP-HRAS^{V12} expression (visualised through GFP fluorescence of the transgene) was barely detectable and no increase of ERK phosphorylation was detected in these lesions, suggesting that either the oncogene was switched off after initial expression, or that UAS:GFP-HRAS^{V12}-expressing cells, which may have initiated abnormal migration/proliferation in the heterotopia, were eliminated so that at the time of the analysis, heterotopias only represented scar-like lesions.

In conclusion, the immunophenotype of these lesions revealed profound differences between heterotopias and tumours, despite their common origin from somatic expression of oncogenes. Inter-tumour variability was found (Fig. 3 and Fig. S3), associated to the different areas of origin of the tumours.

Analysis of global RNA expression established that brain tumours resemble GBMs of the mesenchymal signature, with a strong YAP component.

To establish whether the zebrafish brain tumours developing in our models resemble a specific human molecular subtype, we performed transcriptome analysis by RNA sequencing (RNAseq) of 3 brains of zic:RAS$_{somatic}$ fish, which carried tumour lesions in the telencephalon, diencephalon and IVth ventricle (Fig. S5A) and compared them with tumour free, age matched brains. Using hierarchical clustering on normalised gene expression, the samples clustered in two different groups according to their status (control or tumour, Fig. S5B). We performed an analysis of differential gene expression using DESeq2 (Love et al., 2014), and found 4194 genes differentially expressed (DE) (adjusted p-value < 0.05) in brain tumour samples compared to controls. Of these, 2499 genes were upregulated and 1695 genes were downregulated (Fig. S5C-D).

Next, we evaluated whether the zebrafish brain tumours corresponded to a specific glioma subclass. Verhaak and colleagues identified 840 GBM markers useful to classify glioblastoma in four main subtypes (Verhaak et al., 2010). The same gene signature was later applied to low grade brain tumours (Guan et al., 2014) and to mouse models of brain tumours (Henriquez et al., 2013). We first identified the zebrafish orthologs (Smedley et al., 2015) of the 840 human genes used by Verhaak et al. (Verhaak et al., 2010). Due to the presence of

paralogs in the zebrafish genome (Howe et al., 2013). This resulted in a list of 1135 unique zebrafish Ensembl gene identifiers, which represented 91.31 % of the 840 human GBM markers used by Verhaak et al. (Verhaak et al., 2010) (Table S3). The 4 GBM subtypes were represented by similar numbers of orthologs in zebrafish (Fig. S5E). Using normalised expression data for the zebrafish orthologs of the human markers, we were able to classify the zebrafish brain tumours in one of the 4 GBM subtypes (Fig 4A). Moreover, to further investigate the molecular features of our model, a Gene Set Enrichment Analysis (GSEA) was performed with the whole ranked list of significantly DE genes. Using this enrichment method, the mesenchymal subtype was the only significantly over-represented GBM subclass. We found 82 upregulated zebrafish genes with a normalised enrichment score (NES) of 2.12 and a nominal p-value < 0.001, compared to the classical subclass (up=38, NES=1.16), the proneural subclass (down=38, NES=-0.59) and the neural subclass (down=16, NES=-1.51) (Fig. 4B, Table S3). Interestingly, among the 82 zebrafish orthologs of mesenchymal GBM markers found significantly upregulated in our model, 5 genes were related to YAP signalling: YAP1, WWTR1, TGFBR2, ITGB2 and IQGAP1 (Table S3). This observation prompted us to look at YAP related genes in the total list of 4194 DE genes. To do this, we first created a refined list of 39 zebrafish orthologs of human genes related to YAP signalling, based on literature (Anakk et al., 2013, Kodaka and Hata, 2015, Lim et al., 2014, Mo et al., 2014, Piccolo et al., 2014). Of them, 23 are significantly differentially expressed in the zebrafish brain tumours (adjusted p-value < 0.05, Table S4) which confirmed the mesenchymal nature of our tumour model as YAP/TAZ signalling has been shown to be highly related to the mesenchymal subtype of GBM (Bhat et al., 2011, Orr et al., 2011).

To further investigate the importance of the role of mesenchymal markers, and in particular YAP, we used Qiagen© Ingenuity Pathway Analysis (IPA) which allowed us to identify possible upstream regulators, pathways involved and networks established by the DE genes in the zebrafish tumour model.

Of the 33737 uploaded Ensembl zebrafish IDs, IPA mapped 11896 to human IDs (21841 left unmapped). IPA was able to assess the nature of the model based on the DE genes by returning “Cancer/Neoplasia” as the most prominent Disease/Function in the dataset (Fig. S6A). Additionally, among the deregulated pathways, IPA identified cancer related ones such as Gαq-Signalling, ERK/MAPK-Signalling, PI3K/Akt-Signalling and Hippo-Signalling (Fig. S6B, Table S5). Further, IPA ranks HRAS among the 15 most significant upstream regulators with a p-value of 3.03e-18. To understand which signalling molecules are responsible for the biological effects in our model, we performed a "Regulator Effects

Network" analysis. In this analysis, IPA connects upstream regulators via their target genes to known phenotypic and functional downstream effects. The generated networks are then ranked by the consistency score that is directly proportional to the number of consistent and inconsistent paths and indirectly proportional to the network size. The “Regulatory Effects Network” with by far the highest consistency score is shown in Fig. S6C. This network contains 6 regulators; of those, YAP had the highest interconnectivity, i.e. the highest number of relationships with other genes. Moreover, YAP is the only of the 6 regulators that has a high p-score in the IPA network analysis (Table S6). In this analysis the network headed by HRAS ranked first, whereas the YAP network ranked 12. Finally, the two networks (HRAS and YAP) are highly connected, as shown in Fig. 4C.

All together, these results suggest that YAP is an important regulator in this tumour model and indicate that tumours developing in this model have a mesenchymal gene signature, associated in humans with the most aggressive malignant glioma subtype. A YAP network based on the Ingenuity Pathway Knowledge Database, integrating our RNAseq expression data, is shown in Fig. S6D.

YAP signalling is absent in heterotopia and expression of active YAP promotes development of aggressive brain tumours

After showing the activation of YAP signalling in our model we next investigated the role of YAP activation on tumour formation in this model. To determine the activity of YAP in UAS:GFP-HRAS^{V12} induced tumours we detected the expression levels of YAP through western blot analysis and found a strong increase in total YAP expression in tumours compared to controls and brains with heterotopia (Fig. 5A). Further, we found an increase in YAP target gene expression using qPCR on 22 genes. These data compared well to the NGS data on the same genes, of which 50 % (11 genes) were similarly upregulated, 9 % (2) were strongly upregulated and 41 % (9) were not significantly altered (Figure S7A-B). We chose the 8 most differentially expressed genes (*yap*, *ccnd1*, *ctgfa*, *iqgap1*, *tgfb1a*, *tgfbr2*, *amot*, *itgb2*) and tested this signature on different tumour types and heterotopia which showed overexpression of all 8 genes in tumours of the IVth ventricle and of 6 genes in telencephalic tumours, but no overexpression in heterotopia (Fig. 5B-D). This suggests that Yap target gene expression differentiates tumours versus heterotopia and that some YAP targets (*ctgfa* and *itgb2*) may be tissue or tumour specific.

To further confirm that the 8-gene YAP signature may be a useful molecular diagnostic tool, we analysed human tumours RNA.seq data of 166 GBM and 530 Brain Lower Grade Glioma (LGG) generated by the The Cancer Genome Atlas (TCGA) Research Network (http://cancergenome.nih.gov/). Unsupervised hierarchical clustering (Fig. 5E) demonstrates highly significant segregation of GBMs and LGGs ($p < 10^{-45}$, OR = 28, Fisher Exact Test) supporting that YAP activation is a hallmark of malignant brain cancer and suggesting that this 8-gene signature may provide sufficient information to distinguish high grade from low grade gliomas.

Further, the effect of YAP activation in UAS:GFP-HRAS^{V12} induced tumours was investigated through expression of dominant active YAP (YAP^{S5A}) under control of the UAS promoter. Somatic expression of UAS:YAP^{S5A} alone (zic:YAP$_{somatic}$) induced development of brain tumours (Fig. S8A, B) with YAP target gene expression (Fig. S8C), mixed cell populations (Fig. S8D) and reduced survival comparable to zic:RAS$_{somatic}$ (Fig. S8E). Instead, somatic coexpression of UAS:GFP-HRAS^{V12} and UAS:YAP^{S5A} (zic:RAS,YAP$_{somatic}$, Fig. 6A) promoted tumour development earlier than in zic:RAS$_{somatic}$ (2 weeks, data not shown), and increased proliferation at 3 dpf and 14 dpf (Fig. 6B, C) compared to zic:RAS$_{somatic}$ larvae.

Somatic coexpression of both oncogenes was nearly incompatible with survival allowing only 4 % ± 2.7 % to survive the first month (Fig. 6D). Instead, the few survivors revealed a remarkable increase in the number of fish developing tumours up to 100% and a sharp drop in heterotopia formation down to only 10 % (Fig. 6E). Additionally, UAS:YAP^{S5A} promoted aggressiveness of the developing tumours as they were characterised by strong proliferation and fast dedifferentiation as determined by strong staining for GFAP and nearly complete lack of HU-C staining (Fig. 6F).

Thus, YAP activation is not only co-operating with UAS:GFP-HRAS^{V12} in promoting tumour development but may also function to overcome mechanisms halting tumour development when oncogenes are accidentally expressed in somatic cells during brain development.

Discussion

The progression of pre-malignant developmental lesions to tumours has been proved for several tissues such as colon (Macrae et al., 2009) and pancreas (Aguirre et al., 2003). In the brain, the relation between focal brain developmental disorders and brain cancer has been the subject of several studies aiming at establishing whether a common genetic and developmental origin for these disorders exists in those cases with clear evidences of progression (Aronica and Crino, 2014, Guerrini and Dobyns, 2014, Hevner, 2015). However, for the majority of brain tumours, evidence of a developmental origin of the somatic mutations driving cancer is difficult to obtain. In this study, we have generated a model of progressive brain tumour where the same genetic drivers can give rise to cancer and heterotopia, and identified the signalling pathway that, once activated, promotes tumour development at the expenses of heterotopia. Our model suggests that somatic embryonic mutations activating MAPK/ERK signalling can drive both malformation of brain development and brain tumours, providing that upregulation of YAP signalling is necessary for tumour development.

Somatic mutations in pro-oncogenic factors occurring during development start to be recognised as an important determinant of congenital brain malformation and neurodevelopmental disorders spanning from Proteous syndrome to Neurofibromatosis type I (reviewed in (Poduri et al., 2013). On the other hand, somatic pro-oncogenic mutations occurring in post-developmental stages are often associated with cancer. Several studies have suggested a possible progression between neuro-developmental lesions and brain cancer, especially when the activating mutations induce MAPK/ERK signalling (Hevner, 2015). If a progression is possible from non-cancerous neuro-developmental lesions caused by activating mutations in a pro-oncogenic pathway and brain cancer, then an important question is to identify the mechanisms which restrain affected cells from developing cancer during development, and lead to re-activation of a dormant oncogenic program in case of progression to cancer. However, until now no animal model has been described to allow the investigation of the link between heterotopia and tumour formation.

In our study we have used different oncogenes to generate a model of brain growth disorders in zebrafish. This model shows that RAS/MAPK signalling can simultaneously induce both heterotopia and aggressive brain tumours and that the persistence of the signal differentiates brain tumours from benign developmental lesions. The reduction or absence of GFP-HRAS^{V12} expression in the heterotopia suggests that this could be due to the cells expressing UAS:GFP-

$HRAS^{V12}$ turning off activated Ras after initial expression or undergoing cell death after influencing the ectopic migration of their neighbouring cells. Further studies are needed to clarify this point. In the second part of our study we scrutinised the transcriptional programs activated in those lesions that progress to cancer. We focused on the factors, which appear to be responsible for maintaining ERK signalling in some neural cells, which will form tumours, or shut it down in others, which will develop benign heterotopias. We found that the gene expression profile of RAS/MAPK tumours resembles the mesenchymal GBM signature, reported by Verhaak et al. (Verhaak et al., 2010), which underlines their comparability to the human disease. Additionally, the zebrafish brain tumours expressed a strong YAP component. Yap1 (or YAP) is a transcription co-factor, shut off by the hippo pathway which controls organ size during development (reviewed in Meng et al., 2016). YAP is part of a classic phosphorylation cascade and is activated through different mechanisms to promote growth and migration in cancer (reviewed in (Yu et al., 2015)).

For example pancreatic adenocarcinoma was shown to have a strong YAP component, as KRAS induced acinar-to-ductal metaplasia depends on YAP expression for progression to malignant ductal adenocarcinoma (Zhang et al., 2014). Moreover, cancer cells can use YAP to compensate for loss of mutant KRAS as shown in cell lines and mouse models of pancreatic cancer (Kapoor et al., 2014, Shao et al., 2014). In high grade gliomas, YAP has been shown to be activated especially in aggressive tumour types and its expression tends to correlate with low survival rates (Bhat et al., 2011, Orr et al., 2011). However, the molecular mechanisms behind this correlation are unknown. Analysis of medulloblastoma suggests that upstream regulators of the Hippo pathway control the activation of YAP in brain cancer. Indeed, inhibition of NF2 (encoded by MERLIN) induces nuclear localisation and activation of YAP, that can be rescued by YAP inhibition (Piccolo et al., 2014). Interestingly, the inheritable brain dysplasia Van Maldergen syndrome (VMS; MIM601390) is due to mutations of the Hippo upstream regulators Dchs1 and Fat4, and the phenotype in relevant mouse models can be rescued by YAP inhibition (Cappello et al., 2013).

YAP activity can also be regulated through other mechanisms including interaction with cellular compartments such as the actin cytoskeleton. The actin cytoskeleton has been shown to be crucial for YAP nuclear localisation (Shao et al., 2014), sometimes in cooperation, but more often independently, of the Hippo pathway (Aragona et al., 2013). F-actin translates the mechanical signals from the extra cellular matrix to the cell. As a component of the tumour microenvironment, the extra cellular matrix has a significant impact on the development, progression, and therapy response in tumours (Giussani et al., 2015, Lu et al., 2012). F-actin

can relay its effect on YAP through several mechanisms such as G-protein coupled receptors (GPCRs), which are known to combine the actin cytoskeleton with several signalling pathways (reviewed in (Regue et al., 2013), or IQGAP1, a scaffold protein known to regulate the F-actin and microtubule network and shown to play a pivotal role in a bile acid induced liver cancer through YAP (Anakk et al., 2013). Thus, YAP activation not only correlates with increased proliferation but may promote tumour progression through interactions with the tumour environment. However, the specific mechanism through which YAP translates physical inputs into cancer promoting signals is still to be elucidated.

Our study shows an additional role of YAP in tumour development as expression of dominant active YAP demonstrates its co-operation with oncogenic RAS in the induction of brain cancer instead of neuro-developmental lesions. The mechanisms through which oncogenic RAS induces YAP activation only in some lesions and after some time (3 weeks) from its initial expression, are currently unknown, but may involve a downregulation of members of the ubiquitin ligase complex that target YAP for degradation (SOCS5/6(Hong et al., 2014)), or F-actin through GPCRs or IQGAP1. Further studies will clarify this point.

In contrast to currently available rodent models on brain dysplasia or brain tumours, this zebrafish glioma model provides the advantage of simultaneous development of tumours and heterotopia in a nearly equal ratio, induced by the same oncogene, which enables the analysis of the mechanisms that control the decision in fate and the requirements for progression. Moreover, the model enables time dependent investigation of tumour progression in a living vertebrate on a single cell level. While development of brain tumours was also investigated in other zebrafish models (Ju et al., 2015, Ju et al., 2014, Solin et al., 2015), the model described here provides the advantage of highly frequent development of both heterotopias and neoplastic malignant lesions in more than 80 % of the specimens and very early onset of oncogenic processes, which not only shortens observation times but also allows for efficient screening of therapeutic agents, using prevention of tumour development and tumour progression as read-outs. Further analysis of the model developed in this study can provide an understanding of the mechanisms that promote the progression of benign lesions to malignant tumours and a convenient assay for testing inhibitory treatments that could prevent malignant transformation of developmental brain lesions.

Materials and Methods

Animal housing and line generation

All fish lines were raised and maintained under standard conditions (Westerfield, 2000). Fish with mosaic somatic plasmid expression were generated by co-injection of 0.25 ng/µl DNA (see Table S1) and 0.25 ng/µl mRNA encoding Tol2 transposase into the cell of one-cell-stage embryos. Embryos were kept at 28.5 °C in E3 solution and 0.003 % PTU (1-phenyl-2-thiourea, Sigma Aldrich, Germany) was added to the media at 24 hpf to reduce pigmentation. For line generation, carriers were selected by fluorescence and outcrossed to wildtype strains as adults to generate F0. At least two different F0 per line were analysed, to identify potential insertion effects. No differences between alleles of the same transgenic lines were found, therefore we selected only one of them for further studies.

All Animal experiments were carried out under EU regulations for animal experimentation. The project was approved by the Government of Baden-Württemberg, Regierungspräsidium Karlsruhe, Germany under Aktenzeichen 35-9185.81/G-41/14.

Survival curve

For survival analysis fish were housed in groups of ≤30 and survivors were counted at 0 dpf, 6 dpf, 13 dpf, 24 dpf and 30 dpf. In this and all other comparative analyses, zic:Gal4 fishes/brains were used as controls. The length of these intervals was decided after pilot observations that showed that the majority of the zic:RAS larvae died at around 10-12 dpf. For each curve at least 3 repeats were performed. The total numbers of animals used for the survival curve was 105 (zic:Gal4), 255 (zic:$RAS_{germline}$), 166 (zic:$RAS_{somatic}$), 100 (zic:RAS,$YAP_{somatic}$).

Live imaging of larvae

For live imaging, larvae were anaesthetised with 0.02 % tricaine methanesulfonate (tricaine, Sigma Aldrich, Germany) in E3, embedded in 1 % low melting point (LM) agarose in E3 and imaged with a stereo microscope (LEICA MZTL III), LEICA DFC42 digital camera, LAS V4.5 software or with a confocal microscope (LEICA DMI 4000B) and LAS X software (Leica microsystems, Germany). For repeated imaging, larvae were removed from agarose after each imaging, and housed in 24 well plates as single larvae in E3 mixed with PTU at 28.5 °C until next imaging session.

Brain size quantification

At 3 dpf zic:Gal4 (n = 12) and zic:$RAS_{germline}$ (n = 16) larvae were anesthetised with 0.02 % tricaine in E3, embedded in 1 % LM agarose in E3 and the whole brain imaged from dorsal to ventral using confocal (Leica DMI4000B, Leica microsystems, Germany) under the following settings: objective ACS APO 10.0x0.30 DRY; zoom 1.0 ; z-slice 2 µm; resolution 512x512. Using Matlab each stack of images was assigned a manual threshold and a manual region of interest covering the rostral brain until mid-brain boundary. Using a manual threshold, the RGB images were binarised, followed by a dilation (r = 5), hole filling, erosion (r = 5) and opening (r = 10). The extracted images were cropped using a binary region of interest. The resulting images were used to build a 3D-structure and the volume was quantified (= number of voxels*volume per voxel).

BrdU, H&E, Immunostaining

Fish were killed by anaesthetic overdose (0.04 % tricaine) and brains dissected under a stereomicroscope. All samples were fixed in 4 % PFA for 24 h before paraffin embedding. For proliferation analysis fish were incubated in 10 µM Bromo-deoxy-Uridin (BrdU, Sigma Aldrich, Germany) in E3 24 h prior to sample collection. In 10 larvae per group, total number of $BrdU^+$ cells were counted in coronal sections of the telencephalic areas; in adults $BrdU^+$ cells in tumours, heterotopias or in similar regions of control brains were counted in 2-3 sections of 5 different samples (referring to an area of 0.5 mm^2) given as fraction of total cell number ($DAPI^+$ cells) in that field.

For histological analysis 10 µm serial sections were stained with haematoxylin and eosin (H&E). Images were acquired using a light microscope (Zeiss Axioscope), AxioCam HRc camera and AxioVision SE64 Rel. 4.9.1 software.

For immunohistochemic analysis sections were demasked with a citrate buffer antigen retrieval protocol(Brown and Chirala, 1995) and stained with primary antibodies against glial fibrillary acid protein (GFAP, 1:1000, DAKO, Germany, Z0334), S100β (S100β, 1:1000, DAKO, Germany, Z0311), HU-C (HU-C, 1:200, Life technologies, USA, A21271), phospho-ERK (P-ERK, 1:200, Cell Signalling, USA, 9101S), green fluorescent protein (GFP, mouse 1:500, Millipore, Germany, MAB3580 or rabbit 1:1000, Life technologies, USA, A11122). For staining with the antibody against BrdU (1:500, Cell Signalling, USA, 5292S) sections were additionally treated for 20 min with 2 N HCl. All sections were stained with fluorescent labelled secondary antibodies against rabbit or mouse immunoglobulins (1:200, Life technologies, USA, A11017, A11018, A11070, A11071, A21050, A21070). Images were

acquired using a confocal microscope (LEICA DMI 4000B) and LAS X software (Leica microsystems, Germany).

To obtain the summaries of immunostainings shown in figure 3E/O at least 5 different tumours per region or heterotopias were examined. Number of positive cells or percentage of positive area was evaluated in an area of approximately 0.5 mm^2 in 3 different sections per tumour/heterotopia. The symbols are representative of these counts: less than 5 % positive cells/area = +/-; between 5 and 25 % = +; between 25 and 50 % = ++; over 50 % = +++.

RNA-analysis

All fish were killed by anaesthetic overdose (0.04 % tricaine) and brains of juveniles and adults dissected under a stereomicroscope. Larvae and tissue samples for RNA extraction were collected and lysed in trizol (life technologies, USA) and total RNA extracted with the RNeasy Mini Kit (Qiagen, Germany) following manufacturers protocol. Samples for quantitative PCR (qPCR) analysis were additionally treated with RNA-Free DNase (Quiagen, Germany) for 30 min at RT.

For gene expression analysis via qPCR RNA samples were transcribed to cDNA applying the SuperScript® ViloTM cDNA Synthesis Kit (invitrogen, USA) and qPCR was performed using the Gotaq® qPCR Master Mix (Promega, Germany) following manufacturer's protocol in the StepOnePlus Real-Time PCR System (Applied Biosystems, Germany), with the following setting: 95 °C, 15 min; 40x (95 °C, 15 sec; 60 °C, 30 sec); 95 °C, 15 sec; 60 °C, 1 min; melting curve 0.5 °C per 15 sec to 95 °C. Data were analysed with the StepOne Software v2.3. For normal PCR cDNA samples were diluted 1:10 and 10 µl added to PCR mix (10.5 µl dH2O, 1 µl dNTPs (10 mM mix), 1 µl primer each, 0.5 µl GoTaq® (Promega, Germany), 8 µl 5xbuffer (provided by GoTaq® kit) and amplified in the T100™ Thermal Cycler (BioRad, USA) (95 °C, 5 min; 27x (95 °C, 30 sec; 60 °C, 30 sec; 72 °C, 30 sec) 72 °C, 5 min; 12 °C, ∞). Primer pairs are listed in Table S8.

For next generation sequencing (NGS), the quality of the extracted total RNA samples, using the RNeasy Mini Kit (Qiagen, Germany), was assessed on RNA nanochips (Bioanalyser 2100 Agilent, USA). The libraries were prepared from 1 µg RNA using the Illumina TrueSeq mRNA kit (Illumina, USA) according to the suppliers protocol. The size and the concentration of the libraries were determined with DNA-chip (Bioanalyser 2100 Agilent, USA). A normalised concentration of 8 pM of the libraries was loaded on one lane of a High Through-put sequencing flowcell (Illumina, USA) to generate the clusters, using a cBot (Illumina, USA). The sequencing of the paired-end reads (2 x 50 nucleotides) was done using

an Illumina HiSeq1500 with SBS v3 kits (Illumina, USA). The cluster identification and the base calling were done using RTAv1.13 and the quality of the reads was assessed with CASAVA v1.8.1 (Illumina, USA). The sequencing resulted in an average of 112 millions of reads per sample with, in average, 97% having a quality Phred score greater than 30. The quality of the raw sequencing data was assessed using fastx-toolkit (version 0.0.13) (http://hannonlab.cshl.edu/fastx_toolkit/index.html) and no pre-processing of the data was necessary. The alignment has been done using TopHat2 (version 2.0.11) (Kim et al., 2013) against the assembly Zv9 Ensembl 75 of the Danio rerio genome with the parameters -r 180 --mate-sdt-dev 80 --b2-sensitive --no-novel-junction -a 5 -p 3 --library-type fr-unstranded. The raw gene expression was computed using HTSeq (version 0.5.3p3) (Anders et al., 2015) with --stranded=no --mode=union parameters. The raw sequencing data (fastq files) and the pre-processed data (count files) were submitted to the Gene Expression Omnibus database (http://www.ncbi.nlm.nih.gov/geo/query/acc.cgi?acc=GSE74754). The normalisation of the gene expression and the differential gene expression were both computed using DESeq2 (Love et al., 2014). At this step, the consistency of the biological replicates was tested using hierarchical clustering in a complete mode on Euclidean distances. One control replicate has thus been discarded for the rest of the analysis. The significantly differentially expressed (DE) genes were selected based on an adjusted p-value of less than 0.05, using the Bonferroni multiple testing method. No cut-off was used on the log2 Fold Change. To assess the role of GBM subtype markers of the zebrafish tumour model, the name of the 840 GBM subtype markers, published by Verhaak et al. (Verhaak et al., 2010), were retrieved from TCGA data portal. For the rest of the analysis the markers for GBM subtype were kept but also markers not associated to a specific GBM subtype, labelled 'Non type-specific' (Table S3). The zebrafish orthologs were then found using the Ensembl database and the BioMart portal (Smedley et al., 2015). A curation was applied using 30 % as minimum cut-off for the gene sequence identity or 1 as orthology confidence score cut-off. The list of orthologs was then manually refined for highly important genes. A total of 1135 zebrafish orthologs were found due to the presence of paralogs in the zebrafish genome. The 4 GBM subtypes were similarly represented (Figure S5E). To investigate the involvement of markers of a specific GBM subtype, the pre-ranked algorithm of Gene Set Enrichment Analysis (GSEA) (Subramanian et al., 2005) software package developed by the Broad Institute was used. The significantly DE orthologs of the GBM subtype markers were ranked according to their log2 Fold Change and then used for enrichment with GSEA for the 4 GBM subtype gene sets.

Analysis of human gene expression data

Normalised gene expression data (RNAseqV2) of the signature genes for LGG (n = 530) and GBM (n = 166) were downloaded from cBIOPortal (http://www.cbioportal.org/)(Cerami et al., 2012) by selecting the studies ids “lgg_tcga” and “gbm_tcga”, respectively. The segregation of LGG and GBM samples was tested by Ward’s hierarchical clustering, using (1 - Pearson’s correlation coefficient) as distance measure. Statistical significance of LGG and GBM segregation was estimated by two-sided Fisher Exact test on the two main clusters.

IPA analysis

To predict the effects of gene expression changes in the model QIAGEN’s Ingenuity Pathway Analysis (IPA®, QIAGEN Redwood City, www.qiagen.com/ingenuity) was applied. The complete RNAseq dataset containing the quantitative expression values and corresponding adjusted p-values of all genes comparing zebrafish control brain and zebrafish brain tumour samples was uploaded to IPA and the cut-off for gene analysis set to 0.05. IPA automatically translated zebrafish gene IDs into human gene IDs. For analysis of "Disease or Function" and "Upstream Regulator" the default settings from IPA were applied.

As the RNAseq samples exclusively contained brain tissue the analysis of "Regulatory Effects Network" was restricted accordingly by removing liver, kidney, lung, skeletal, cardiac and sensory organ effects from the analysis.

For the analysis of "Network" the default settings from IPA were applied, which restricts the outcome to the 25 most significant "Networks". These are constructed between genes of the dataset according to the number of known interactions with other genes, assuming that the number of interactions correlates with the biological relevance of the gene product. The Networks are sorted by "Score" which reflects their interconnectivity.

Western Blot

Fish were killed by anaesthetic overdose (0.04 % tricaine) and their brains dissected under a stereomicroscope. The samples were homogenized in sample buffer (5 % Glycerol, 1.7 % SDS, 60 mM TrisHCl pH 6.8, 0.01 % EDTA) containing protease inhibitors (cOmplete, Roche, Germany) and phosphatase inhibitors (phosphoStop, Roche, Germany). Equal amounts (20-50 mg) of the total extract were separated on 10 % acrylamide gels and transferred to a PVDF membrane applying Trans-Blot® Turbo™ RTA Transfer Kit, PVDF (BioRad, USA) and Trans-Blot® Turbo™ Transfer System machine (BioRad, USA). The

membrane was blocked in 2 % BSA and incubated with the following antibodies over night (P-Erk (1:200, Cell Signalling, USA, 9101S), YAP (1:200, Cell Signalling, USA, 4912)). After washing, the membrane was incubated 1.5 h at RT with horseradish peroxidase-conjugated goat anti-mouse IgG (Dako, Germany, P0447) or goat anti-rabbit IgG (Dako, Germany, P0448), washed again and activated with Pierce® ECL Western Blotting Substrate (Thermo Scientific, USA) system. For reuse, the membrane was treated with Restore™ Western Blot Stripping Buffer (Thermo Scientific, USA) according to the supplier's protocol. For normalisation, antibodies against total Erk (1:200, Cell Signalling, 9102) or actin (1:5000, Neomarkers-Fremont, USA, ACTN05) were used on stripped membranes.

Cloning

For the generation of transgenes expressing UAS:BRAF^{V600E}, UAS:Xmrk, UAS:EGFR $_{\text{splice variant III}}$ (shortened in $_{\text{vIII}}$), UAS:Yap^{S5A} and UAS:lifeact-GFP we used different strategies. As a backbone (vector) we used pT2MUASMCS (a kind gift from Koichi Kawakami), which contains a Tol2 based flanking cassette for genomic integration, and five UAS repeats before the multiple cloning site. We used conventional cloning of blunt fragments in the EcoRV cloning site of the pT2MUASMCS vector, followed by 5' and 3' sequencing to check orientation and integrity of the insert. Inserts were GFP tagged using gateway recombination with pEntry clones of the Tol2kit (Kwan et al., 2007) before being cloned into pT2MUASMCS. For UAS controlled myristoylated AKT1 we used gateway recombination to clone a 5xUAS:Akt1:5xUAS:BFP construct into pDEST Tol2 CG2.

The plasmids containing the different oncogenes that were used as templates in Gateway cloning were kind gifts of the following labs: BRAF^{V600E} (Liz Patton, Edinburgh, UK); Xmrk (Manfred Schartl, Würzburg, Germany), pcDNA3 Myr HA Akt1 was a gift from William Sellers (Addgene plasmid # 9008) (Ramaswamy et al., 1999), MSCV-XZ066-EGFRvIII was a gift from Alonzo Ross (Addgene plasmid # 20737) (Li et al., 2009), YAP^{S5A} (Sirio Dupont, Padova, Italy). Lifeact-GFP (Riedl et al., 2008) was obtained from the authors.

3D visualization

CLARITY procedure

Whole-dissected adult brains were fixed in freshly prepared ice-cold methanol-free paraformaldehyde (PFA) 4 % (wt/vol) in 0.01 M PBS (pH 7.4) overnight at 4 °C. Samples were then infused in a pre-cooled solution of (4 °C) freshly prepared hydrogel monomers (0.01 PBS, 0.25 % VA-044 initiator (wt/vol), 5 % dimethyl sulfoxide (vol/vol), 1 % PFA

(wt/vol), 4 % acrylamide (wt/vol) and 0.0025 % bis-acrylamide (wt/vol)) for 2 days at 4 °C. After degassing the samples the hydrogel polymerisation was triggered by replacing atmospheric oxygen with nitrogen in a desiccation chamber for 3 hours at 37 °C. Samples were cleaned from superfluous hydrogel and transferred into embedding cassettes for lipid clearing. Passive lipid clearing was performed at 40 °C for 8 days in the clearing solution (8 % SDS (wt/vol), 0.2 M boric acid, pH adjusted to 8.5) under gentle agitation. Subsequently the samples were thoroughly washed in 0.01 M PBS, tween 0.1 % (wt/vol) (PBSt) at room temperature with gentle agitation for 2 days.

Immunostaining of clarified samples

CLARITY-processed brains were incubated in blocking solution (0.01 M PBS, 0.1 % tween 20 (vol/vol), 1 % Triton X100 (vol/vol), 10 % dimethyl sulfoxide (vol/vol), 10 % normal goat serum (vol/vol), 0.05 M glycine) overnight at 4 °C. Subsequently samples were incubated in staining solution (0.01 M PBS, 0.1 % tween 20 (vol/vol), 0.1 % Triton X100 (vol/vol), 10 % dimethyl sulfoxide (vol/vol), 2 % normal goat serum (vol/vol), 0.05 % azide (vol/vol)) with primary antibody (chicken anti-GFP, Avès Labs, 1:400) for 7 days at room temperature under gentle agitation. After four washing steps in PBSt, samples were incubated in staining solution with secondary antibody (goat anti-chicken Alexa Fluor 488, Invitrogen, 1:400) for 7 days at room temperature. Samples were washed for 2 days in PBSt and stained with 1 µM DiIC18(3) solution (DiI Stain, Molecular Probes).

Imaging in high refractive index solution

A fructose-based high refractive index medium (fruM) was prepared as follows: 70 % fructose (wt/vol), 20 % DMSO (wt/vol) in 0.002 M PBS, 0.005 % Sodium azide (wt/vol). The refractive index of the solution was adjusted to 1.4571 using a refractometer (Kruss).

In preparation of the imaging the samples were incubated in 50 % (vol/vol) fruM for 6 h and finally incubated in fruM for at least 12 h. For imaging, samples were mounted in 1 % (wt/vol) low melting point agarose and covered with fruM. Whole-mount brain fluorescence was recorded with a Leica TCS SP8 two-photon microscope. Fluorescence was excited using a mode locked Ti:Sapphire laser (Chameleon, Coherent) at 770 nm with the Leica HC FLUOTAR L 25x/1.00 IMM motCorr objective. Non-descanned detectors with 525/50 and 585/40 bandpass filters were used for data acquisition. As the specimens are significantly bigger than the field of view of the used objective tiled scanning with a voxel size of 0.9x0.9x1 (µm) or 1.7x1.7x1.7 (µm) was applied.

Image treatment and visualization

In preparation of the visualisation the image stacks was converted from their native 12 bit lif-format to series of 8 bit-pngs using CLAHE (Zuiderfeld, 1994) for ImageJ (Schneider et al., 2012) as implemented in fiji (Schindelin et al., 2012). The implementation is described online (Saalfeld, http://fiji.sc/Enhance_Local_Contrast_%28CLAHE%29). The parameters for CLAHE were empirically tested and set to a blocksize of 127, 256 bins and a slope of 3 (default values). While reducing the bit depth from 12 bit to 8 bit fiji's CLAHE plugin enhances the contrast and intensity of the weak signals significantly while not over-saturating strong signals. By this a significant contrast enhancement and data reduction can be achieved. Manual segmentation and 3D rendering was performed with amira (www.fei.com) using a combination of the 'Segmentation Editor', 'Voltex', 'Volume Rendering' and 'Surface View' modules.

Statistics

For statistical analysis GraphPad Prism 6 was used applying unpaired Student’s t-tests and Bonferroni correction. Values are given in mean ± standard deviation (STD).

Acknowledgements

For generously providing us with plasmids we deeply thank Liz Patton ($BRAF^{V600E}$), Manfred Schartl (Xmrk), William Sellers (pcDNA3 Myr HA Akt1), Alonzo Ross (MSCV-XZ066-EGFRvIII), Sirio Dupont (YAP^{S5A}) and Koichi Kawakami (pT2MUASMCS). We thank Sabrina Burkart for excellent technical support and M. Cominelli for help with some of the histological stainings. The fish lines were housed by the EZRC (Karlsruhe, Germany).

The results on human data are in whole based upon data generated by the TCGA Research Network: http://cancergenome.nih.gov/.

Competing Interests statement

None.

Author Contributions

M. Mione and M. Mayrhofer conceived the study, performed most of the experiments, analysed the results and wrote the manuscript. M. Reischl performed the brain size calculation. V. Gourain performed the bioinformatics analysis. A. Jenett, P. Affaticati and J-S. Joly performed the CLARITY protocol, analysed the data and generated the related images. M. Benelli and F. Demichelis performed the computational analysis of human glioma/GBM data. P.L. Poliani stained and analysed histopathological zebrafish samples. D. Sieger cloned the $EGFR_{vIII}$ and the AKT-BFP plasmids. All Authors commented on the manuscript.

Funding

This study was funded by grant AICR 11-06024 to M. Mione from Worldwide Cancer Research. M. Mayrhofer acknowledges the support through the Studienstiftung des deutschen Volkes and FAZIT. F. Demichelis acknowledges the support of US National Cancer Institute (R01 CA125612 to F.D.) This work has benefited from the facilities and expertise of TEFOR - Investissement d'avenir - ANR-II-INBS-0014.

Data availability

Accession codes: Sequencing data have been deposited in GEO at National Center for Biotechnology Information under the accession number GSE74754.

References

AGUIRRE, A. J., BARDEESY, N., SINHA, M., LOPEZ, L., TUVESON, D. A., HORNER, J., REDSTON, M. S. & DEPINHO, R. A. 2003. Activated Kras and Ink4a/Arf deficiency cooperate to produce metastatic pancreatic ductal adenocarcinoma. *Genes & development,* 17**,** 3112-26.

ANAKK, S., BHOSALE, M., SCHMIDT, V. A., JOHNSON, R. L., FINEGOLD, M. J. & MOORE, D. D. 2013. Bile acids activate YAP to promote liver carcinogenesis. *Cell reports,* 5**,** 1060-9.

ANDERS, S., PYL, P. T. & HUBER, W. 2015. HTSeq--a Python framework to work with high-throughput sequencing data. *Bioinformatics,* 31**,** 166-9.

ARAGONA, M., PANCIERA, T., MANFRIN, A., GIULITTI, S., MICHIELIN, F., ELVASSORE, N., DUPONT, S. & PICCOLO, S. 2013. A mechanical checkpoint controls multicellular growth through YAP/TAZ regulation by actin-processing factors. *Cell,* 154**,** 1047-59.

ARONICA, E. & CRINO, P. B. 2014. Epilepsy related to developmental tumors and malformations of cortical development. *Neurotherapeutics : the journal of the American Society for Experimental NeuroTherapeutics,* 11**,** 251-68.

ARUGA, J. 2004. The role of Zic genes in neural development. *Molecular and cellular neurosciences,* 26**,** 205-21.

BALLESTER, R., MARCHUK, D., BOGUSKI, M., SAULINO, A., LETCHER, R., WIGLER, M. & COLLINS, F. 1990. The NF1 locus encodes a protein functionally related to mammalian GAP and yeast IRA proteins. *Cell,* 63**,** 851-9.

BARKOVICH, A. J., GUERRINI, R., KUZNIECKY, R. I., JACKSON, G. D. & DOBYNS, W. B. 2012. A developmental and genetic classification for malformations of cortical development: update 2012. *Brain : a journal of neurology,* 135**,** 1348-69.

BHAT, K. P., SALAZAR, K. L., BALASUBRAMANIYAN, V., WANI, K., HEATHCOCK, L., HOLLINGSWORTH, F., JAMES, J. D., GUMIN, J., DIEFES, K. L., KIM, S. H., et al. 2011. The transcriptional coactivator TAZ regulates mesenchymal differentiation in malignant glioma. *Genes & development,* 25**,** 2594-609.

BLUMCKE, I., THOM, M., ARONICA, E., ARMSTRONG, D. D., VINTERS, H. V., PALMINI, A., JACQUES, T. S., AVANZINI, G., BARKOVICH, A. J., BATTAGLIA, G., et al. 2011. The clinicopathologic spectrum of focal cortical dysplasias: a consensus classification proposed by an ad hoc Task Force of the ILAE Diagnostic Methods Commission. *Epilepsia,* 52**,** 158-74.

BROWN, R. W. & CHIRALA, R. 1995. Utility of microwave-citrate antigen retrieval in diagnostic immunohistochemistry. *Modern pathology : an official journal of the United States and Canadian Academy of Pathology, Inc,* 8**,** 515-20.

CAPPELLO, S., GRAY, M. J., BADOUEL, C., LANGE, S., EINSIEDLER, M., SROUR, M., CHITAYAT, D., HAMDAN, F. F., JENKINS, Z. A., MORGAN, T., et al. 2013. Mutations in genes encoding the cadherin receptor-ligand pair DCHS1 and FAT4 disrupt cerebral cortical development. *Nature genetics,* 45**,** 1300-8.

CERAMI, E., GAO, J., DOGRUSOZ, U., GROSS, B. E., SUMER, S. O., AKSOY, B. A., JACOBSEN, A., BYRNE, C. J., HEUER, M. L., LARSSON, E., et al. 2012. The cBio cancer genomics portal: an open platform for exploring multidimensional cancer genomics data. *Cancer discovery,* 2**,** 401-4.

CHAICHANA, K. L., MCGIRT, M. J., LATERRA, J., OLIVI, A. & QUINONES-HINOJOSA, A. 2010. Recurrence and malignant degeneration after resection of adult hemispheric low-grade gliomas. *Journal of neurosurgery,* 112**,** 10-7.

CICHOWSKI, K. & JACKS, T. 2001. NF1 tumor suppressor gene function: narrowing the GAP. *Cell,* 104**,** 593-604.

COURCHESNE, E., KARNS, C. M., DAVIS, H. R., ZICCARDI, R., CARPER, R. A., TIGUE, Z. D., CHISUM, H. J., MOSES, P., PIERCE, K., LORD, C., et al. 2001. Unusual brain growth patterns in early life in patients with autistic disorder: an MRI study. *Neurology,* 57**,** 245-54.

CRINO, P. B. 2013. Evolving neurobiology of tuberous sclerosis complex. *Acta neuropathologica,* 125**,** 317-32.

DISTEL, M., WULLIMANN, M. F. & KOSTER, R. W. 2009. Optimized Gal4 genetics for permanent gene expression mapping in zebrafish. *Proceedings of the National Academy of Sciences of the United States of America,* 106**,** 13365-70.

DYMENT, D. A., SAWYER, S. L., CHARDON, J. W. & BOYCOTT, K. M. 2013. Recent advances in the genetic etiology of brain malformations. *Current neurology and neuroscience reports,* 13**,** 364.

EVANS, D. G., HOWARD, E., GIBLIN, C., CLANCY, T., SPENCER, H., HUSON, S. M. & LALLOO, F. 2010. Birth incidence and prevalence of tumor-prone syndromes: estimates from a UK family genetic register service. *American journal of medical genetics. Part A,* 152A**,** 327-32.

FOMCHENKO, E. I. & HOLLAND, E. C. 2006. Mouse models of brain tumors and their applications in preclinical trials. *Clinical cancer research : an official journal of the American Association for Cancer Research,* 12**,** 5288-97.

GIUSSANI, M., MERLINO, G., CAPPELLETTI, V., TAGLIABUE, E. & DAIDONE, M. G. 2015. Tumor-extracellular matrix interactions: Identification of tools associated with breast cancer progression. *Seminars in cancer biology,* 35**,** 3-10.

GRAJKOWSKA, W., KOTULSKA, K., JURKIEWICZ, E. & MATYJA, E. 2010. Brain lesions in tuberous sclerosis complex. Review. *Folia neuropathologica / Association of Polish Neuropathologists and Medical Research Centre, Polish Academy of Sciences,* 48**,** 139-49.

GRINBERG, I. & MILLEN, K. J. 2005. The ZIC gene family in development and disease. *Clinical genetics,* 67**,** 290-6.

GUAN, X., VENGOECHEA, J., ZHENG, S., SLOAN, A. E., CHEN, Y., BRAT, D. J., O'NEILL, B. P., DE GROOT, J., YUST-KATZ, S., YUNG, W. K., et al. 2014. Molecular subtypes of glioblastoma are relevant to lower grade glioma. *PloS one,* 9**,** e91216.

GUERRINI, R. & DOBYNS, W. B. 2014. Malformations of cortical development: clinical features and genetic causes. *The Lancet. Neurology,* 13**,** 710-26.

HENRIQUEZ, N. V., FORSHEW, T., TATEVOSSIAN, R., ELLIS, M., RICHARD-LOENDT, A., ROGERS, H., JACQUES, T. S., REITBOECK, P. G., PEARCE, K., SHEER, D., et al. 2013. Comparative expression analysis reveals lineage relationships between human and murine gliomas and a dominance of glial signatures during tumor propagation in vitro. *Cancer research,* 73**,** 5834-44.

HEVNER, R. F. 2015. Brain overgrowth in disorders of RTK-PI3K-AKT signaling: a mosaic of malformations. *Seminars in perinatology,* 39**,** 36-43.

HO, A. L., KOCH, M. J., TANAKA, S., EICHLER, A. F., BATCHELOR, T. T., TANBOON, J., LOUIS, D. N., CAHILL, D. P., CHI, A. S. & CURRY, W. T., JR. 2016. Impact of histopathological transformation and overall survival in patients with progressive anaplastic glioma. *Journal of clinical neuroscience : official journal of the Neurosurgical Society of Australasia,* 31**,** 99-105.

HONG, X., NGUYEN, H. T., CHEN, Q., ZHANG, R., HAGMAN, Z., VOORHOEVE, P. M. & COHEN, S. M. 2014. Opposing activities of the Ras and Hippo pathways converge on regulation of YAP protein turnover. *The EMBO journal,* 33**,** 2447-57.

HOWE, K., CLARK, M. D., TORROJA, C. F., TORRANCE, J., BERTHELOT, C., MUFFATO, M., COLLINS, J. E., HUMPHRAY, S., MCLAREN, K., MATTHEWS, L., et al. 2013. The zebrafish reference genome sequence and its relationship to the human genome. *Nature,* 496**,** 498-503.

JOHANSSON, G., ANDERSSON, U. & MELIN, B. 2015. Recent developments in brain tumor predisposing syndromes. *Acta oncologica***,** 1-11.

JONES, D. T., GRONYCH, J., LICHTER, P., WITT, O. & PFISTER, S. M. 2012. MAPK pathway activation in pilocytic astrocytoma. *Cellular and molecular life sciences : CMLS,* 69**,** 1799-811.

JONES, D. T., KOCIALKOWSKI, S., LIU, L., PEARSON, D. M., BACKLUND, L. M., ICHIMURA, K. & COLLINS, V. P. 2008. Tandem duplication producing a novel oncogenic BRAF fusion gene defines the majority of pilocytic astrocytomas. *Cancer research,* 68**,** 8673-7.

JU, B., CHEN, W., ORR, B. A., SPITSBERGEN, J. M., JIA, S., EDEN, C. J., HENSON, H. E. & TAYLOR, M. R. 2015. Oncogenic KRAS promotes malignant brain tumors in zebrafish. *Molecular cancer,* 14**,** 18.

JU, B., CHEN, W., SPITSBERGEN, J. M., LU, J., VOGEL, P., PETERS, J. L., WANG, Y. D., ORR, B. A., WU, J., HENSON, H. E., et al. 2014. Activation of Sonic hedgehog signaling in neural progenitor cells promotes glioma development in the zebrafish optic pathway. *Oncogenesis,* 3**,** e96.

JUNG, I. H., LEEM, G. L., JUNG, D. E., KIM, M. H., KIM, E. Y., KIM, S. H., PARK, H. C. & PARK, S. W. 2013. Glioma is formed by active Akt1 alone and promoted by active Rac1 in transgenic zebrafish. *Neuro-oncology,* 15**,** 290-304.

KAPOOR, A., YAO, W., YING, H., HUA, S., LIEWEN, A., WANG, Q., ZHONG, Y., WU, C. J., SADANANDAM, A., HU, B., et al. 2014. Yap1 activation enables bypass of oncogenic Kras addiction in pancreatic cancer. *Cell,* 158**,** 185-97.

KIM, D., PERTEA, G., TRAPNELL, C., PIMENTEL, H., KELLEY, R. & SALZBERG, S. L. 2013. TopHat2: accurate alignment of transcriptomes in the presence of insertions, deletions and gene fusions. *Genome biology,* 14**,** R36.

KODAKA, M. & HATA, Y. 2015. The mammalian Hippo pathway: regulation and function of YAP1 and TAZ. *Cellular and molecular life sciences : CMLS,* 72**,** 285-306.

KWAN, K. M., FUJIMOTO, E., GRABHER, C., MANGUM, B. D., HARDY, M. E., CAMPBELL, D. S., PARANT, J. M., YOST, H. J., KANKI, J. P. & CHIEN, C. B. 2007. The Tol2kit: a multisite gateway-based construction kit for Tol2 transposon transgenesis constructs. *Developmental dynamics : an official publication of the American Association of Anatomists,* 236**,** 3088-99.

LI, L., DUTRA, A., PAK, E., LABRIE, J. E., 3RD, GERSTEIN, R. M., PANDOLFI, P. P., RECHT, L. D. & ROSS, A. H. 2009. EGFRvIII expression and PTEN loss synergistically induce chromosomal instability and glial tumors. *Neuro-oncology,* 11**,** 9-21.

LIM, B., PARK, J. L., KIM, H. J., PARK, Y. K., KIM, J. H., SOHN, H. A., NOH, S. M., SONG, K. S., KIM, W. H., KIM, Y. S., et al. 2014. Integrative genomics analysis reveals the multilevel dysregulation and oncogenic characteristics of TEAD4 in gastric cancer. *Carcinogenesis,* 35**,** 1020-7.

LIU, L., BACKLUND, L. M., NILSSON, B. R., GRANDER, D., ICHIMURA, K., GOIKE, H. M. & COLLINS, V. P. 2005. Clinical significance of EGFR amplification and the aberrant EGFRvIII transcript in conventionally treated astrocytic gliomas. *Journal of molecular medicine,* 83**,** 917-26.

LOUIS, D.N., PERRY, A., REIFENBERGER, G., VON DEIMLING, A., FIGARELLA-BRANGER, D., CAVENEE, W.K., OHGAKI, H., WIESTLER, O.D., KLEIHUES, P., ELLISON, D.W. 2016. The 2016 World Health Organization Classification of Tumors of the Central Nervous System: a summary. *Acta Neuropathol*, 131, 803-20.

LOVE, M. I., HUBER, W. & ANDERS, S. 2014. Moderated estimation of fold change and dispersion for RNA-seq data with DESeq2. *Genome biology,* 15**,** 550.

LU, P., WEAVER, V. M. & WERB, Z. 2012. The extracellular matrix: a dynamic niche in cancer progression. *The Journal of cell biology,* 196**,** 395-406.

MACRAE, F., DU SART, D. & NASIOULAS, S. 2009. Familial adenomatous polyposis. *Best practice & research. Clinical gastroenterology,* 23**,** 197-207.

MARIN-VALENCIA, I., GUERRINI, R. & GLEESON, J. G. 2014. Pathogenetic mechanisms of focal cortical dysplasia. *Epilepsia,* 55**,** 970-8.

MENG, Z., MOROISHI, T. & GUAN, K. L. 2016. Mechanisms of Hippo pathway regulation. *Genes & development,* 30**,** 1-17.

MO, J. S., PARK, H. W. & GUAN, K. L. 2014. The Hippo signaling pathway in stem cell biology and cancer. *EMBO reports,* 15**,** 642-56.

NETWORK, T. C. G. A. R. 2008. Comprehensive genomic characterization defines human glioblastoma genes and core pathways. *Nature,* 455**,** 1061-8.

OHGAKI, H. & KLEIHUES, P. 2007. Genetic pathways to primary and secondary glioblastoma. *The American journal of pathology,* 170**,** 1445-53.

OHGAKI, H. & KLEIHUES, P. 2009. Genetic alterations and signaling pathways in the evolution of gliomas. *Cancer science,* 100**,** 2235-41.

ORR, B. A., BAI, H., ODIA, Y., JAIN, D., ANDERS, R. A. & EBERHART, C. G. 2011. Yes-associated protein 1 is widely expressed in human brain tumors and promotes glioblastoma growth. *Journal of neuropathology and experimental neurology,* 70**,** 568-77.

PALMINI, A., PAGLIOLI, E. & SILVA, V. D. 2013. Developmental tumors and adjacent cortical dysplasia: single or dual pathology? *Epilepsia,* 54 Suppl 9**,** 18-24.

PATIL, C. G., NUNO, M., ELRAMSISY, A., MUKHERJEE, D., CARICO, C., DANTIS, J., HU, J., YU, J. S., FAN, X., BLACK, K. L., et al. 2013. High levels of phosphorylated MAP kinase are associated with poor survival among patients with glioblastoma during the temozolomide era. *Neuro-oncology,* 15**,** 104-11.

PENMAN, C. L., FAULKNER, C., LOWIS, S. P. & KURIAN, K. M. 2015. Current Understanding of BRAF Alterations in Diagnosis, Prognosis, and Therapeutic Targeting in Pediatric Low-Grade Gliomas. *Frontiers in oncology,* 5**,** 54.

PICCOLO, S., DUPONT, S. & CORDENONSI, M. 2014. The biology of YAP/TAZ: hippo signaling and beyond. *Physiological reviews,* 94**,** 1287-312.

PODURI, A., EVRONY, G. D., CAI, X. & WALSH, C. A. 2013. Somatic mutation, genomic variation, and neurological disease. *Science,* 341**,** 1237758.

RAMASWAMY, S., NAKAMURA, N., VAZQUEZ, F., BATT, D. B., PERERA, S., ROBERTS, T. M. & SELLERS, W. R. 1999. Regulation of G1 progression by the PTEN tumor suppressor protein is linked to inhibition of the phosphatidylinositol 3-kinase/Akt pathway. *Proceedings of the National Academy of Sciences of the United States of America,* 96**,** 2110-5.

REGUE, L., MOU, F. & AVRUCH, J. 2013. G protein-coupled receptors engage the mammalian Hippo pathway through F-actin: F-Actin, assembled in response to Galpha12/13 induced RhoA-GTP, promotes dephosphorylation and activation of the YAP oncogene. *BioEssays : news and reviews in molecular, cellular and developmental biology*, 35**,** 430-5.

REUSS, D. & VON DEIMLING, A. 2009. Hereditary tumor syndromes and gliomas. *Recent results in cancer research. Fortschritte der Krebsforschung. Progres dans les recherches sur le cancer*, 171**,** 83-102.

RIEDL, J., CREVENNA, A. H., KESSENBROCK, K., YU, J. H., NEUKIRCHEN, D., BISTA, M., BRADKE, F., JENNE, D., HOLAK, T. A., WERB, Z., et al. 2008. Lifeact: a versatile marker to visualize F-actin. *Nature methods*, 5**,** 605-7.

SANTORIELLO, C., GENNARO, E., ANELLI, V., DISTEL, M., KELLY, A., KOSTER, R. W., HURLSTONE, A. & MIONE, M. 2010. Kita driven expression of oncogenic HRAS leads to early onset and highly penetrant melanoma in zebrafish. *PloS one*, 5**,** e15170.

SANTOS, M. V., DE OLIVEIRA, R. S. & MACHADO, H. R. 2014. Approach to cortical dysplasia associated with glial and glioneuronal tumors (FCD type IIIb). *Child's nervous system : ChNS : official journal of the International Society for Pediatric Neurosurgery*, 30**,** 1869-74.

SCHINDELIN, J., ARGANDA-CARRERAS, I., FRISE, E., KAYNIG, V., LONGAIR, M., PIETZSCH, T., PREIBISCH, S., RUEDEN, C., SAALFELD, S., SCHMID, B., et al. 2012. Fiji: an open-source platform for biological-image analysis. *Nature methods*, 9**,** 676-82.

SCHNEIDER, C. A., RASBAND, W. S. & ELICEIRI, K. W. 2012. NIH Image to ImageJ: 25 years of image analysis. *Nature methods*, 9**,** 671-5.

SHAO, D. D., XUE, W., KRALL, E. B., BHUTKAR, A., PICCIONI, F., WANG, X., SCHINZEL, A. C., SOOD, S., ROSENBLUH, J., KIM, J. W., et al. 2014. KRAS and YAP1 converge to regulate EMT and tumor survival. *Cell*, 158**,** 171-84.

SMEDLEY, D., HAIDER, S., DURINCK, S., PANDINI, L., PROVERO, P., ALLEN, J., ARNAIZ, O., AWEDH, M. H., BALDOCK, R., BARBIERA, G., et al. 2015. The BioMart community portal: an innovative alternative to large, centralized data repositories. *Nucleic acids research*, 43**,** W589-98.

SOLIN, S. L., SHIVE, H. R., WOOLARD, K. D., ESSNER, J. J. & MCGRAIL, M. 2015. Rapid tumor induction in zebrafish by TALEN-mediated somatic inactivation of the retinoblastoma1 tumor suppressor rb1. *Scientific reports*, 5**,** 13745.

STYLLI, S. S., LUWOR, R. B., WARE, T. M., TAN, F. & KAYE, A. H. 2015. Mouse models of glioma. *Journal of clinical neuroscience : official journal of the Neurosurgical Society of Australasia*, 22**,** 619-26.

SUBRAMANIAN, A., TAMAYO, P., MOOTHA, V. K., MUKHERJEE, S., EBERT, B. L., GILLETTE, M. A., PAULOVICH, A., POMEROY, S. L., GOLUB, T. R., LANDER, E. S., et al. 2005. Gene set enrichment analysis: a knowledge-based approach for interpreting genome-wide expression profiles. *Proceedings of the National Academy of Sciences of the United States of America,* 102**,** 15545-50.

THOM, M., MARTINIAN, L., PARNAVELAS, J. G. & SISODIYA, S. M. 2004. Distribution of cortical interneurons in grey matter heterotopia in patients with epilepsy. *Epilepsia,* 45**,** 916-23.

TOHMA, Y., GRATAS, C., BIERNAT, W., PERAUD, A., FUKUDA, M., YONEKAWA, Y., KLEIHUES, P. & OHGAKI, H. 1998. PTEN (MMAC1) mutations are frequent in primary glioblastomas (de novo) but not in secondary glioblastomas. *Journal of neuropathology and experimental neurology,* 57**,** 684-9.

VERHAAK, R. G., HOADLEY, K. A., PURDOM, E., WANG, V., QI, Y., WILKERSON, M. D., MILLER, C. R., DING, L., GOLUB, T., MESIROV, J. P., et al. 2010. Integrated genomic analysis identifies clinically relevant subtypes of glioblastoma characterized by abnormalities in PDGFRA, IDH1, EGFR, and NF1. *Cancer cell,* 17**,** 98-110.

WESTERFIELD, M. 2000. *The Zebrafish Book. A Guide for the Laboratory Use of Zebrafish (Danio rerio),* Eugene, University of Oregon Press.

WINDEN, K. D., YUSKAITIS, C. J. & PODURI, A. 2015. Megalencephaly and Macrocephaly. *Seminars in neurology,* 35**,** 277-87.

WONG, M. & ROPER, S. N. 2015. Genetic animal models of malformations of cortical development and epilepsy. *Journal of neuroscience methods*.

YU, F. X., ZHAO, B. & GUAN, K. L. 2015. Hippo Pathway in Organ Size Control, Tissue Homeostasis, and Cancer. *Cell,* 163**,** 811-28.

ZHANG, W., NANDAKUMAR, N., SHI, Y., MANZANO, M., SMITH, A., GRAHAM, G., GUPTA, S., VIETSCH, E. E., LAUGHLIN, S. Z., WADHWA, M., et al. 2014. Downstream of Mutant KRAS, the Transcription Regulator YAP Is Essential for Neoplastic Progression to Pancreatic Ductal Adenocarcinoma. *Science signaling,* 7**,** ra42.

ZUIDERFELD, K. 1994. Contrast limited adaptive histogram equalization. *In:* HECKBERT, P. S. (ed.) *Graphics Gems IV.* San Diego, Ca, USA: Morgan Kaufmann.

Figures

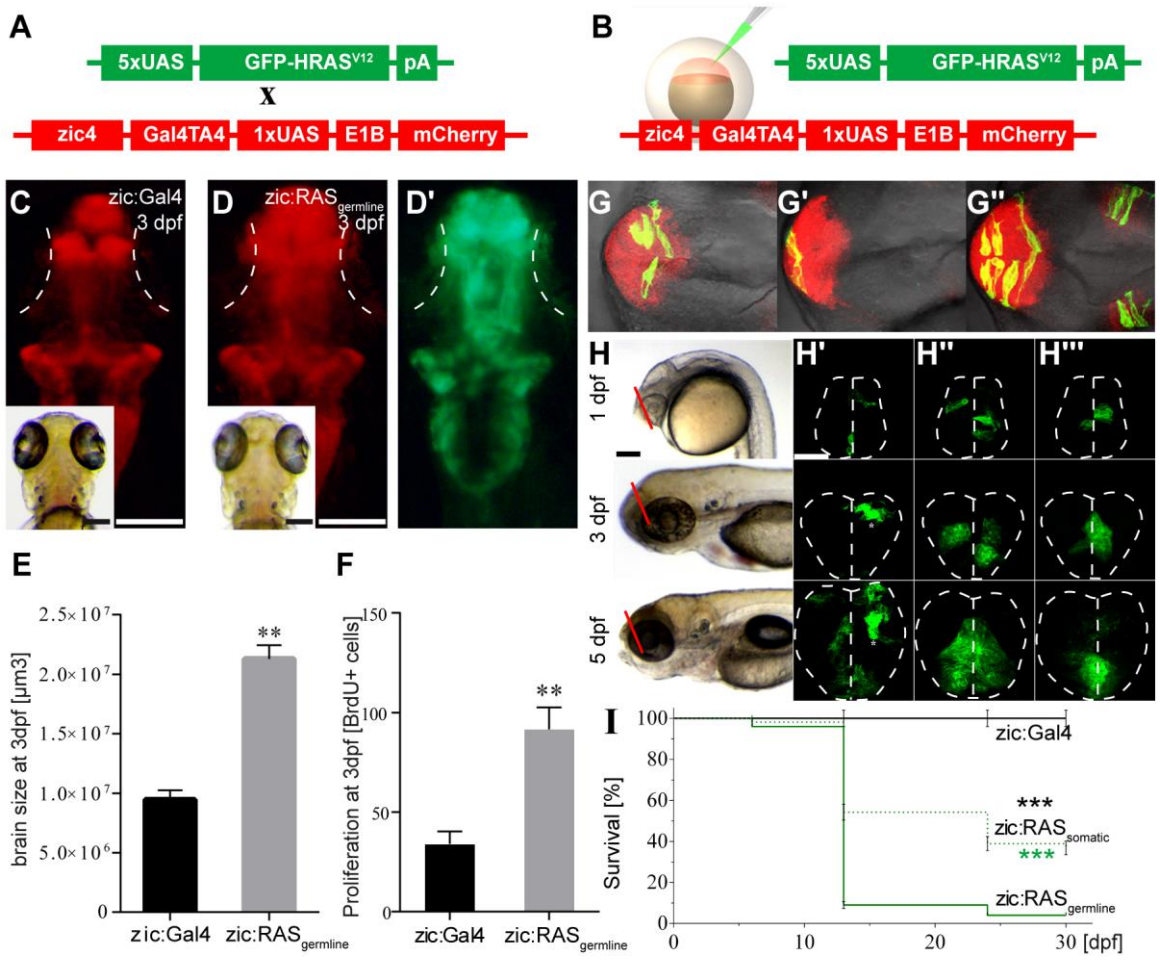

Figure 1: Oncogenic RAS induces proliferation of neural progenitor cells, clonal expansion and reduced survival.

A-B) Schematic representation of tumour induction through (**A**) the cross between zebrafish lines carrying the indicated transgenes or (**B**) the injection of the oncogenic construct (green) into zic:Gal4 embryos to express *UAS:GFP-HRAS^{V12}* specifically in the brain. **C-D**) Dorsal view of representative 3 dpf images of larvae showing the telencephalon in a control larva (**C** = zic:Gal4, mCherry expression) compared to that of an oncogenic larva (**D** = zic:RAS$_{germline}$, mCherry expression, **D'** = zic:RAS$_{germline}$, UAS:GFP-HRAS^{V12} expression), white dotted lines mark the eyes. **E**) Quantification of brain size reveals a doubling in size of the zic:RAS$_{germline}$ expressing tissue. **F**) Counting of BrdU positive cells in the telencephalon of 3 dpf larvae reveals doubling in the number of proliferating cells in zic:RAS$_{germline}$ versus zic:Gal4 controls. **G-G"**) Dorsal view of three 1 dpf zic:RAS$_{somatic}$ larvae showing individual clones expressing UAS:GFP-HRAS^{V12}. **H-H"'**) Lateral bright field and coronal confocal images of

the telencephalon of three live zic:$RAS_{somatic}$ larvae (plane of focus indicated by red lines in **H**) at 1 dpf, 3 dpf and 5 dpf revealing clonal expansion of oncogene-expressing cells in the same larvae from 1 to 5 dpf. **I**) Survival curve of zic:$RAS_{somatic}$ larvae (green dashed line; #=166) compared to zic:Gal4 controls (black line, black asterisk; #=105) and zic:$RAS_{germline}$ larvae (green solid line, green asterisk; #=255). Data are represented as mean ± SD. Scale bars: **C-D** = 500 µm; **F** = 500 µm; **F‘** = 50 µm; **p-value<0.03; ***p-value<0.001.

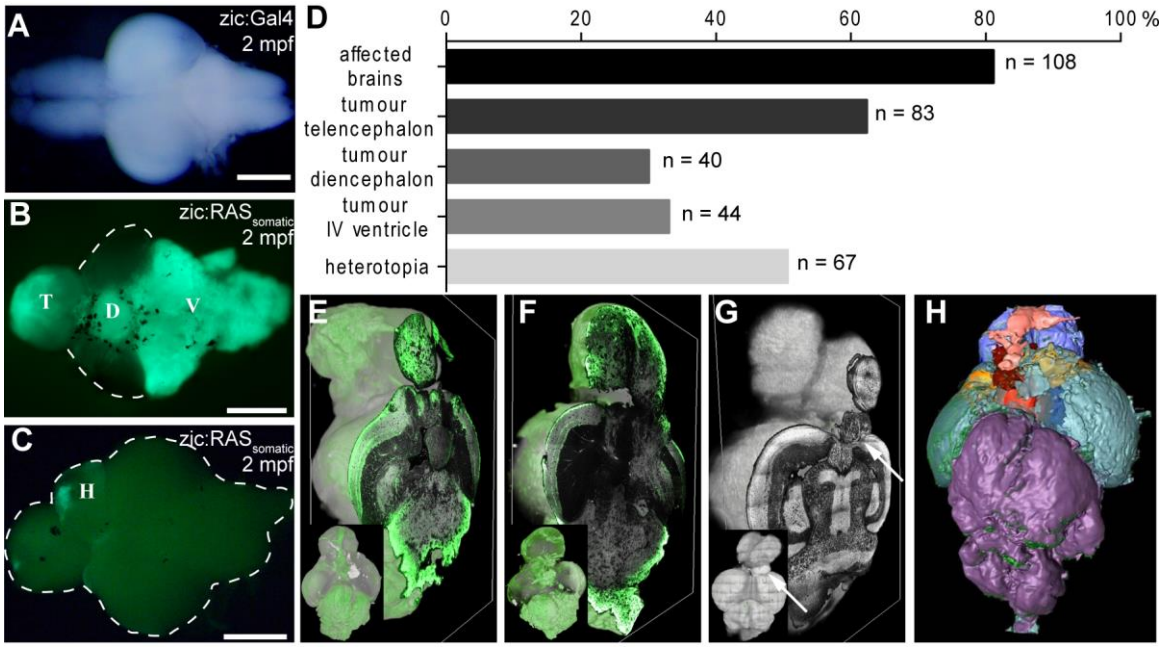

Figure 2: Somatic expression of oncogenic RAS induces tumour development and heterotopia.

A-C) Fluorescence images of 2 mpf zebrafish brains of zic:Gal4 (**A**) and zic:$RAS_{somatic}$ fish (**B-C**) showing (**A**) a control brain, (**B**) tumours in the telencephalon ("T"), diencephalon ("D") and IVth ventricle region ("V") and (**C**) heterotopia ("H"). **D**) Graph representing the frequency of different lesions due to induction of UAS:GFP-$HRAS^{V12}$ expression (n = 134, of which "T" = 83, "D" = 40, "V" = 44, "H" = 67). **E-G**) Volume rendering of 3D reconstructions of two brains with tumours (**E-F**, green areas) and a brain with heterotopia (**G**, white arrow) shown as dorsal view (inset) and 1 sagittal section (large image). **H**) 3D reconstruction and volume rendering of a brain showing different tumour expansions (colour coded according to histological and anatomical features and GFP expression). Scale bars: **A-C** = 2 mm.

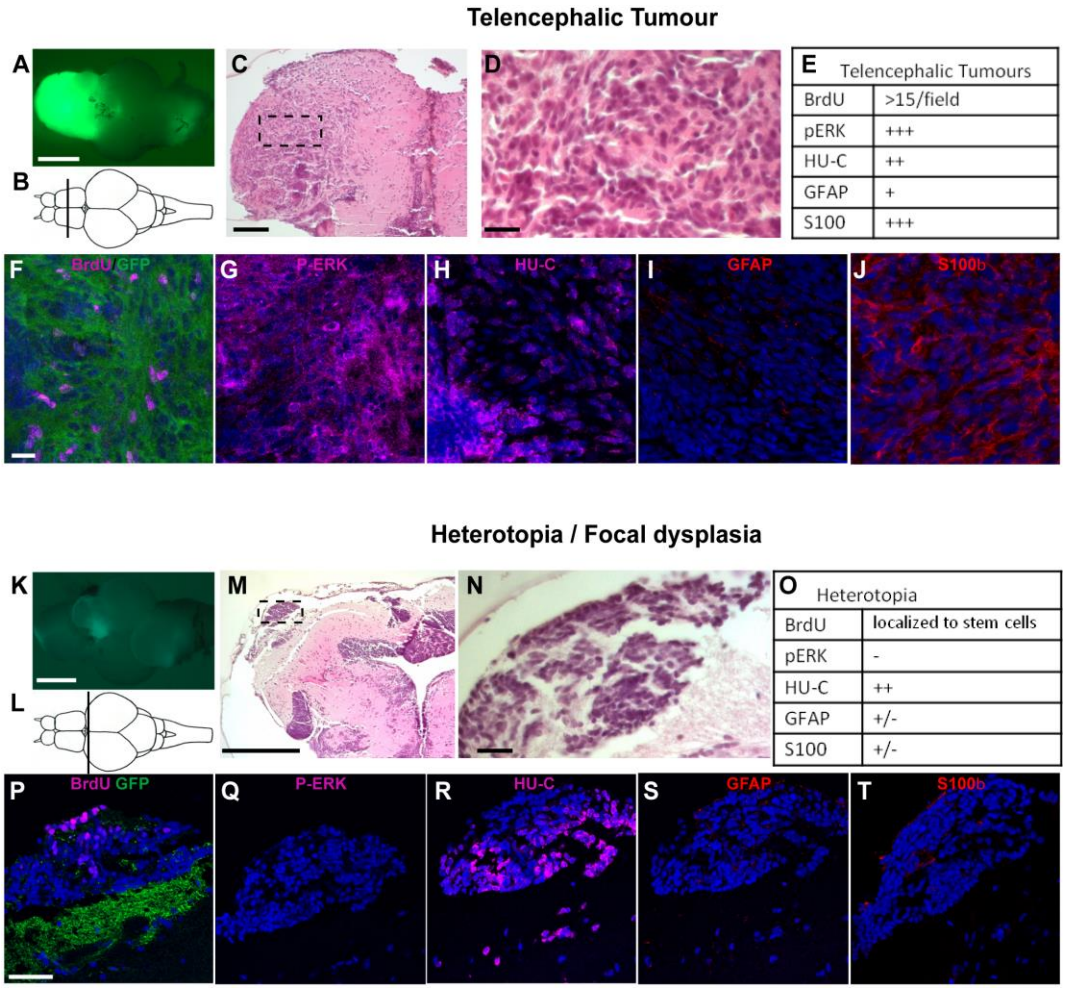

Figure 3: Histological and immunological appearance of telencephalic tumour and heterotopia.

A) Representative telencephalic tumour in zic:RAS$_{somatic}$ fish. **B**) Schematic drawing, indicating the position of the sections shown in **F-J**. **C**) H&E stained section, boxed area indicates enlargement shown in **D**. **E**) Summary of the immunohistochemical observations related to telencephalic tumours. **F-J**) Immunostaining of telencephalic tumour sections stained as indicated. DAPI as counterstaining is in blue. **K**) Representative heterotopia in zic:RAS$_{somatic}$ fish. **L**) Schematic drawing, indicating the position of the sections shown in **P-T**. **M**) H&E stained section, boxed area indicates enlargement shown in **N**. **O**) Summary of the immunohistochemical observations related to heterotopia. **P-T**) Immunostaining of telencephalic tumour sections stained as indicated. DAPI as counterstaining is in blue. Scale bars: **A**, **K** = 2 mm; **C**, **M** = 200 µm; **D**, **F-J**, **N**, **P-T** = 25 µm.

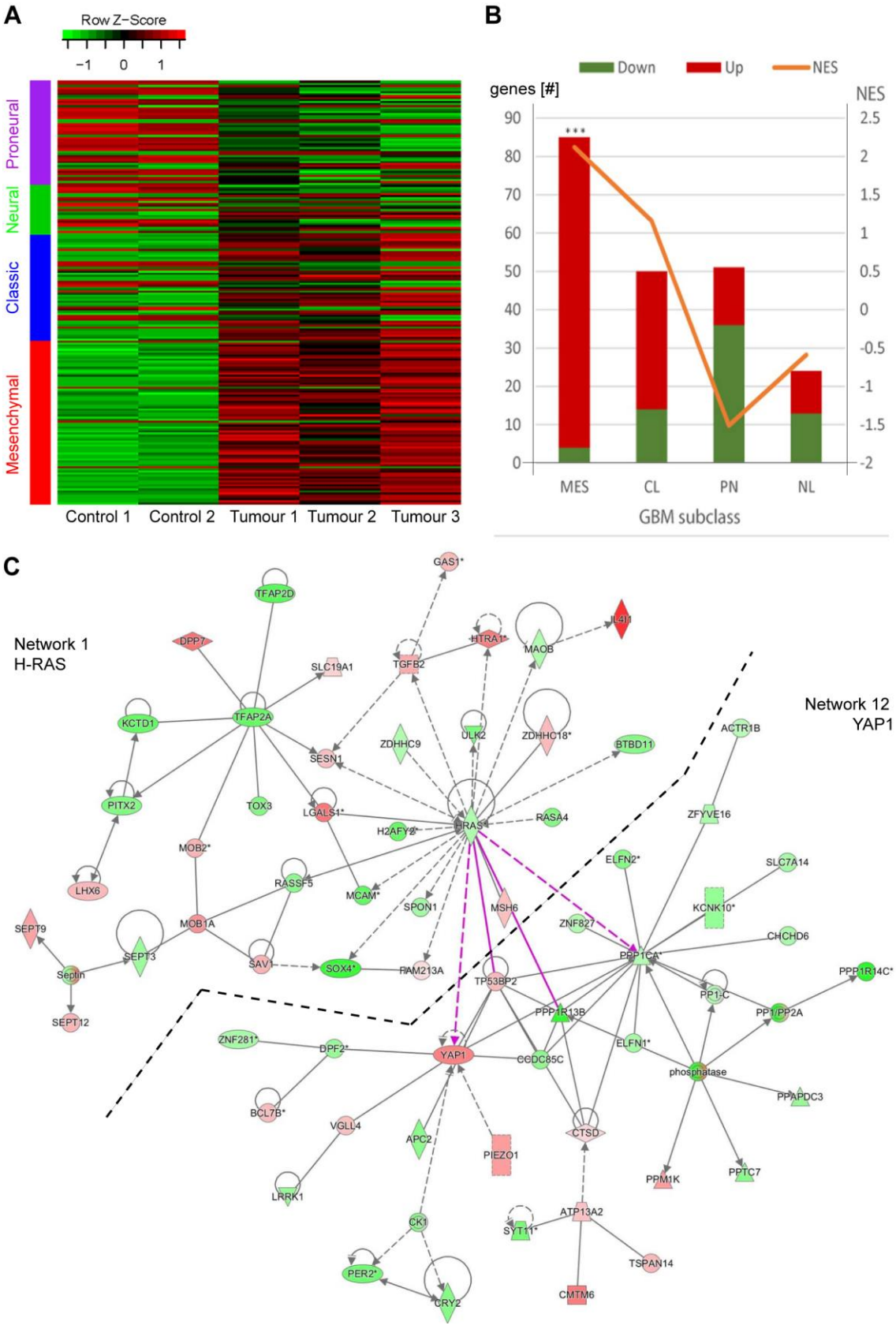
A
Row Z-Score
−1
0
1
Proneural
Neural
Classic
Mesenchymal
Control 1
Control 2
Tumour 1
Tumour 2
Tumour 3
B
Down
Up
NES
genes [#]
NES
***
MES
CL
PN
NL
GBM subclass
C
Network 1
H-RAS
Network 12
YAP1
GAS1*
TFAP2D
DPP7
HTRA1*
IL4I1
MAOB
SLC19A1
TGFB2
KCTD1
TFAP2A
ZDHHC9
ULK2
ZDHHC18*
BTBD11
ACTR1B
SESN1
PITX2
TOX3
LGALS1*
HRAS*
RASA4
ZFYVE16
H2AFY2*
MOB2*
ELFN2*
SLC7A14
LHX6
RASSF5
MCAM*
SPON1
MSH6
KCNK10*
SEPT9
MOB1A
ZNF827
CHCHD6
SEPT3
SAV1
SOX4*
FAM213A
PPP1CA*
Septin
TP53BP2
PPP1R14C*
PP1-C
SEPT12
PPP1R13B
PP1/PP2A
ZNF281*
DPF2*
YAP1
CCDC85C
ELFN1*
phosphatase
BCL7B*
PPAPDC3
VGLL4
APC2
CTSD
PIEZO1
PPM1K
PPTC7
LRRK1
CK1
ATP13A2
SYT11*
PER2*
TSPAN14
CRY2
CMTM6

Figure 4: The zebrafish brain tumours resemble mesenchymal subtypes of human GBMs.

A) Heatmap comparing gene expression data of brains of zic:Gal4 (Control 1-2) and zic:$RAS_{somatic}$ fish (Tumour 1-3) representing the normalised expression of the 248 significantly differentially expressed zebrafish orthologs of human GBM markers (adjusted p-value<0.05). After row scaling the zebrafish genes visually group into human GBM subclasses. **B**) The Gene Set Enrichment Analysis (GSEA) on the orthologs of the GBM human markers shows that only the mesenchymal (MES) subclass is significantly enriched (FDR<0.001), associated to 82 zebrafish genes (orthologs of 85 GBM human markers). The classical (CL) subclass is associated to 53 zebrafish genes (50 GBM human markers), the proneural (PL) subclass to 52 zebrafish genes (51 GBM human markers) and the neural (NL) subclass to 27 zebrafish genes (24 GBM human markers). The orange line identifies the normalised enrichment score (NES). **C**) IPA Network analysis suggests a close relation between HRAS and YAP in this tumour model as it connects HRAS (network1) with YAP (network12) via 4 connections (red lines).

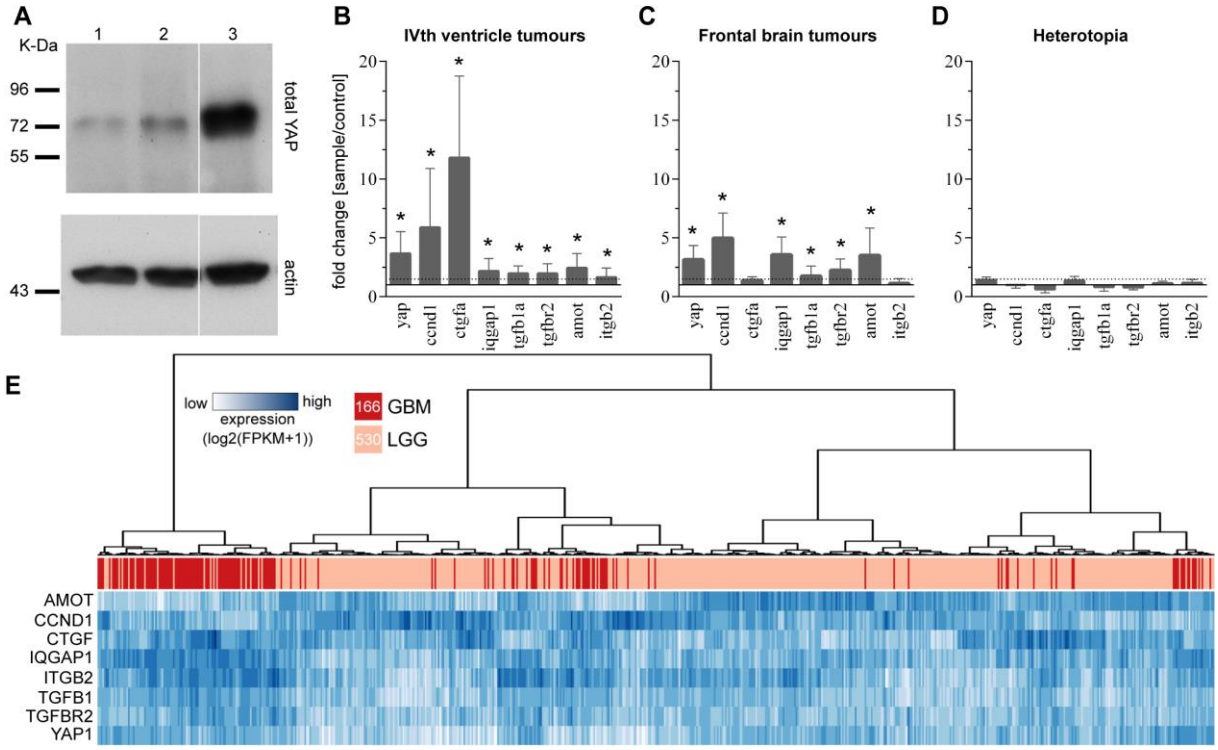

Figure 5: A simple YAP signature distinguishes tumours from benign lesions.

A) Western blot analysis shows increased YAP in tumour versus controls and heterotopia (1 = control brain; 2 = heterotopia; 3 = tumour (UAS:GFP-HRAS$^{V12}_{germline}$). **B-D**) Expression of 8 YAP-target genes showing upregulation in tumours of the (**B**) IVth ventricle (n = 6) and (**C**) frontal brain (n = 6) and no upregulation in (**D**) heterotopia (n = 5) when compared to control brains. **E)** Hierarchical clustering of the gene expression data of the 8-gene YAP signature on 166 GBM (dark pink) and 530 LGG (light pink) samples using (1 - Pearson's correlation) as distance measure. Gene expression is reported as Fragments Per Kilobase of transcript per Million fragments mapped (FPKM).

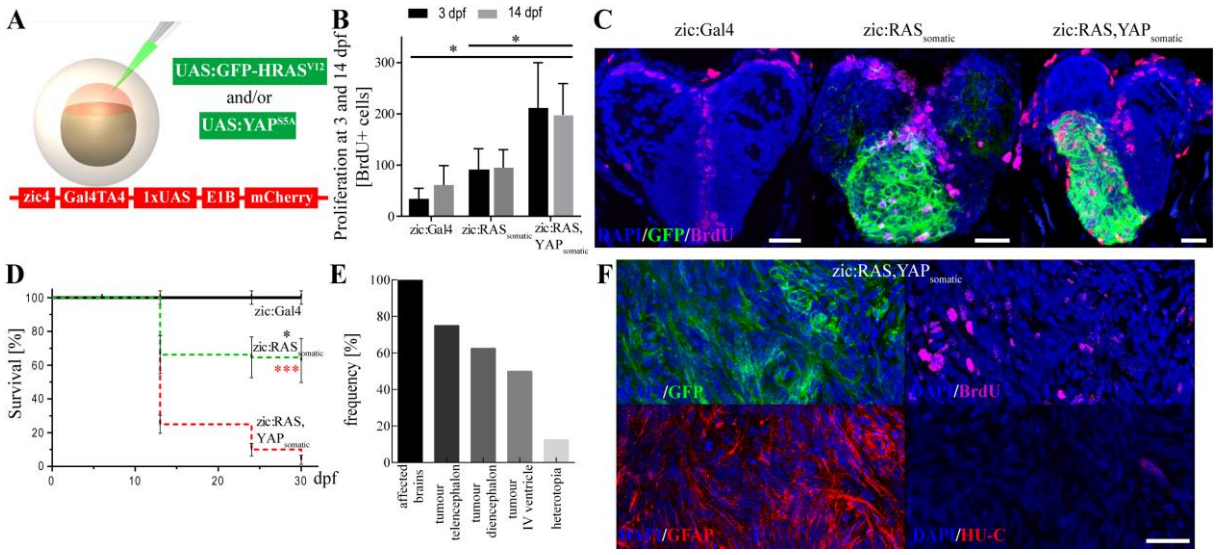

Figure 6: YAP activation promotes tumour growth.

A) Schematic representation of tumour induction through the co-injection of oncogenic constructs (green) into zic:Gal4 embryos. **B**) Quantification of BrdU positive cells in the telencephalon of 3 and 14 dpf juveniles reveals doubling in the number of proliferating cells in zic:RAS,YAP$_{somatic}$ fish compared to zic:RAS$_{somatic}$ fish and zic:Gal4 control fish. **C**) Confocal image of 14 dpf fish showing BrdU expression (magenta) in zic:Gal4, zic:RAS$_{somatic}$ and zic:RAS,YAP$_{somatic}$. **D**) Survival rate of zic:RAS$_{somatic}$ (green dashed line; #=166) compared to zic:Gal4 (black solid line, black asterisk; #=105) and zic:RAS,YAP$_{somatic}$ (red dashed line, red asterisks; #=100). **E**) Graph representing the frequency of different lesions due to zic:RAS,YAP$_{somatic}$ expression as determined by stereomicroscopic analysis with tumours in telencephalon ("T"), diencephalon ("D") and IVth ventricle ("V") and heterotopia ("H"). **F**) Immunostaining for GFP, BrdU, GFAP and HU-C of zic:RAS,YAP$_{somatic}$ fish. Data are represented as mean ± SD. Scale bars: **C**, **F** = 20 µm; *p-value<0.05; ***p-value<0.001.

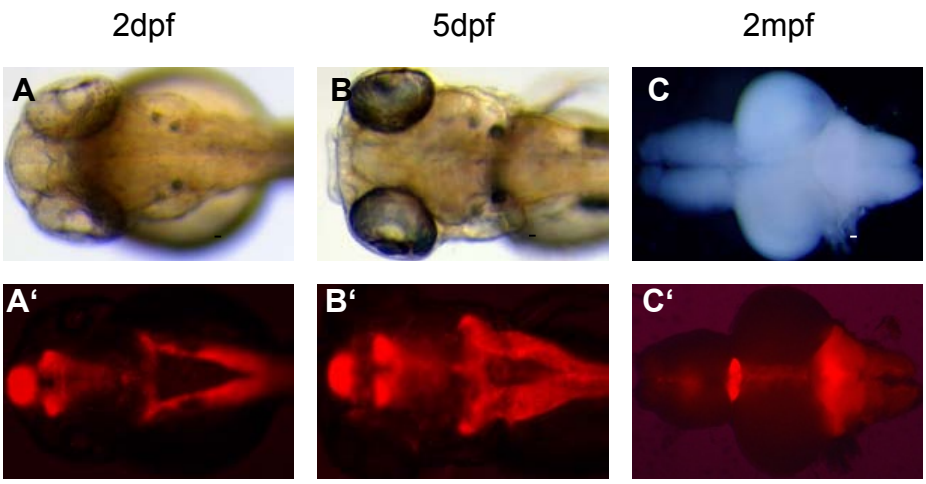

Figure S1: Gal4 expression pattern in control fish (zic:Gal4).
A-C) Visualisation of zic:Gal4 expression during zebrafish development as indicated. Bright field images (**A-C**) and Gal4 expression (**A‘-C‘**) visualised through mCherry fluorescence at 2 dpf (**A**), 5 dpf (**B**) and in the brain at 2 mpf (**C**). Scale bars: **A-B** = 500 µm, **C** = 2 mm.

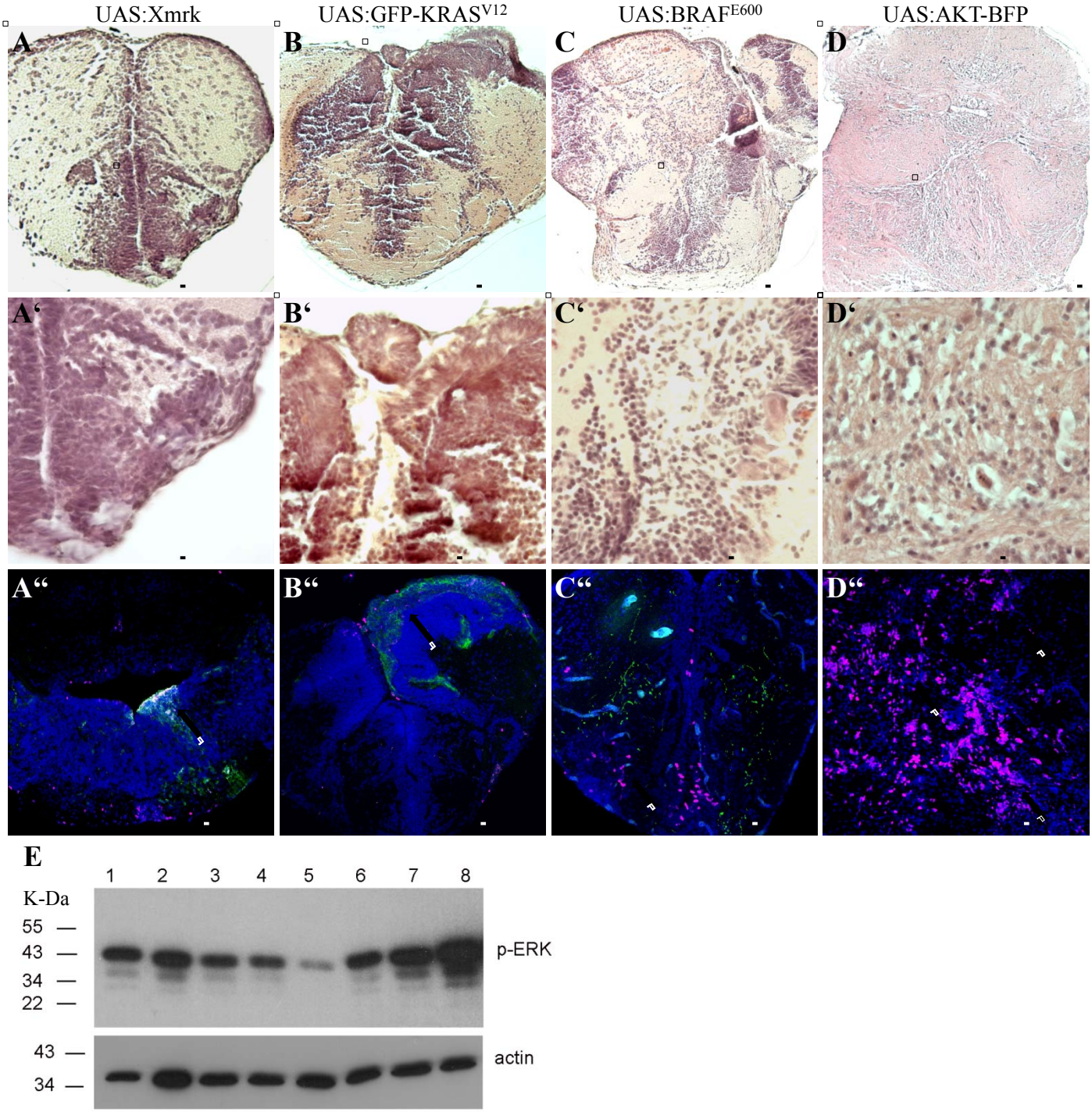

Figure S2: *Tumours can be induced by different oncogenes.*
A-D) H&E staining of lesions induced by somatic expression of different oncogenes. Boxed area indicates enlargement shown in **A'-D'**, respectively. **A"-D"**) Immunostaining for BrdU of lesions induced by somatic expression of different oncogenes. Arrows point at lesions. **E**) Western blot showing the levels of phosphorylated ERK (P-ERK) and actin in control brain (lane 1), heterotopia (lane 2), zic:EGFR$_{VIIIsomatic}$ (lane 3), zic:Xmrk$_{somatic}$ (lane 4), zic:AKT-BFP$_{somatic}$ (lane 5), zic:BRAF^{E600}$_{somatic}$ (lane 6), zic:GFP-KRAS^{V12}$_{somatic}$ (lane 7) and zic:GFP-HRAS^{V12}$_{somatic}$ (land 8). Scale bars: **A-C** = 100 µm; **D** = 1 mm; **A'-D'** = 50 µm; **A"-D"** = 100 µm.

Figure S3

Dorsal Diencephalic Tumour

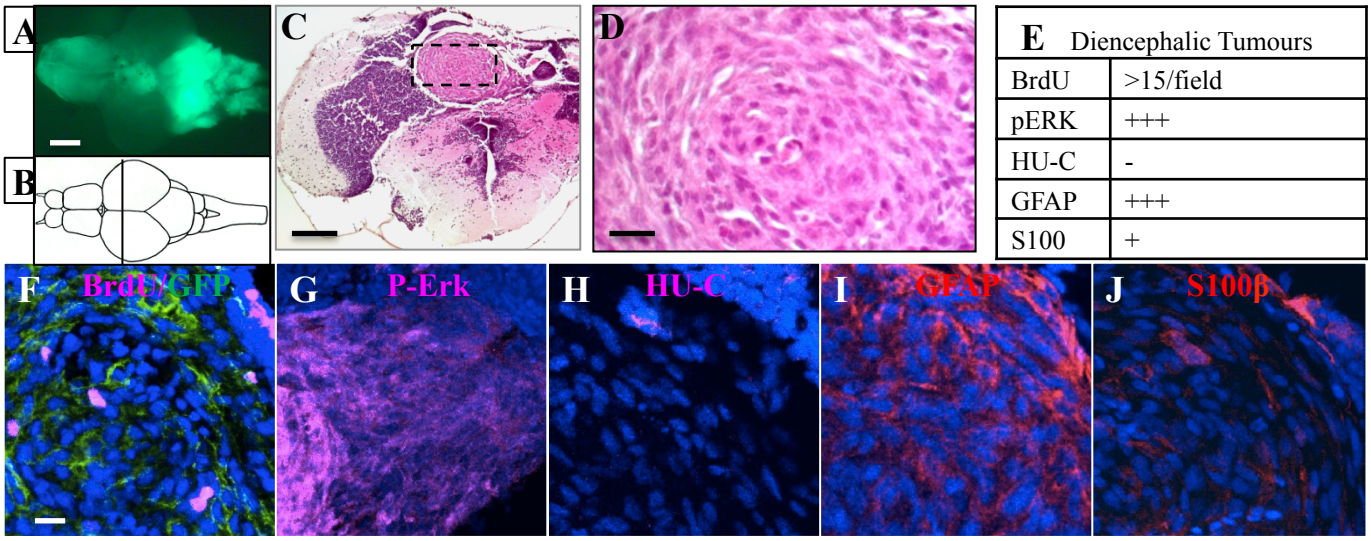

E Diencephalic Tumours	
BrdU	>15/field
pERK	+++
HU-C	-
GFAP	+++
S100	+

IVth Ventricle Tumour

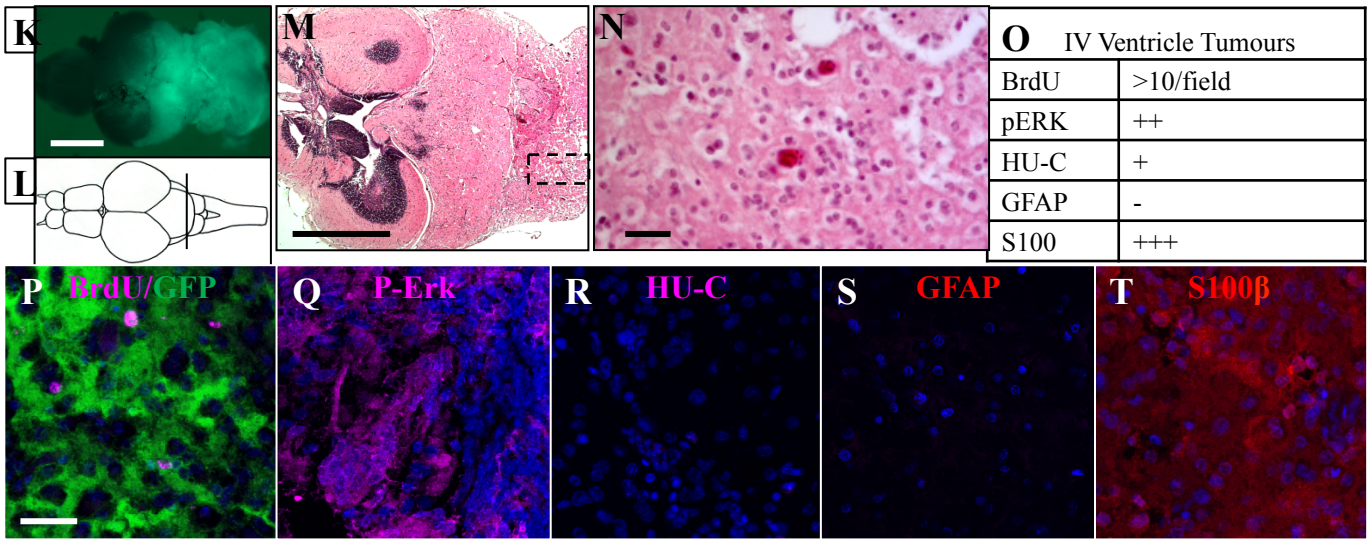

O IV Ventricle Tumours	
BrdU	>10/field
pERK	++
HU-C	+
GFAP	-
S100	+++

Figure S3: *Histological and immunological appearance of IVth ventricle and diencephalic tumours.* **A**) Representative diencephalic tumour in zic:RAS$_{somatic}$ fish. **B**) Schematic drawing, indicating the position of the sections shown in **F-J**. **C**) H&E stained section, boxed area indicates enlargement shown in **D**. **E**) Summary of the immunohistochemical observations related to diencephalic tumours. **F-J**) Immunostaining of heterotopia sections stained as indicated. **K**) Representative IVth ventricle tumour in zic:RAS$_{somatic}$ fish. **L**) Schematic drawing, indicating the position of the sections shown in **P-T**. **M**) H&E stained section, boxed area indicates enlargement shown in **N**. **O**) Summary of the immunohistochemical observations related to IV ventricle tumours. **P-T**) Immunostaining of IVth ventricle tumour sections stained as indicated. Scale bars: **A, K**= 2 mm; **C, M**=200 μm; **D, F-J, N, P-T** = 25 μm.

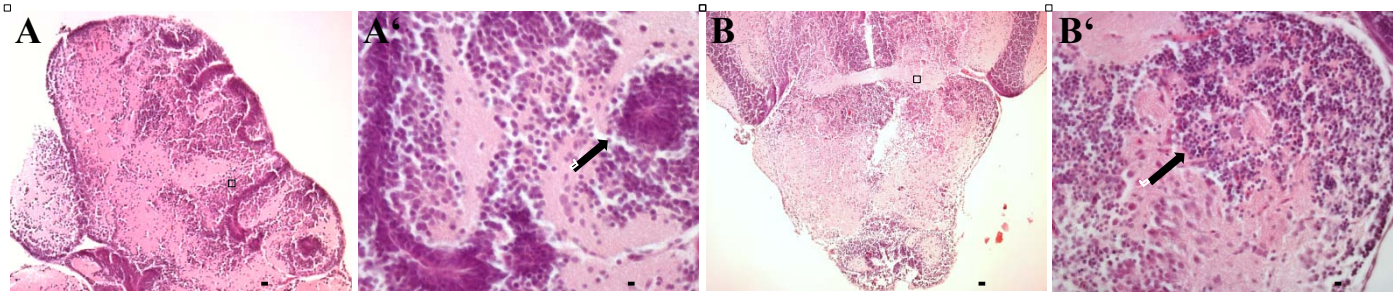

Figure S4: *Heterotopia occurs also in telencephalon and cerebellum.*
A) Representative telencephalic heterotopia in zic:$RAS_{somatic}$, boxed area indicates enlargement shown in **A'**. **B**) Representative IVth ventricle heterotopia zic:$RAS_{somatic}$, boxed area indicates enlargement shown in **B'**. Black arrows point at abnormally localised neural cells (heterotopia). Scale bars: **A, B** = 100 µm; **A', B'** = 20 µm.

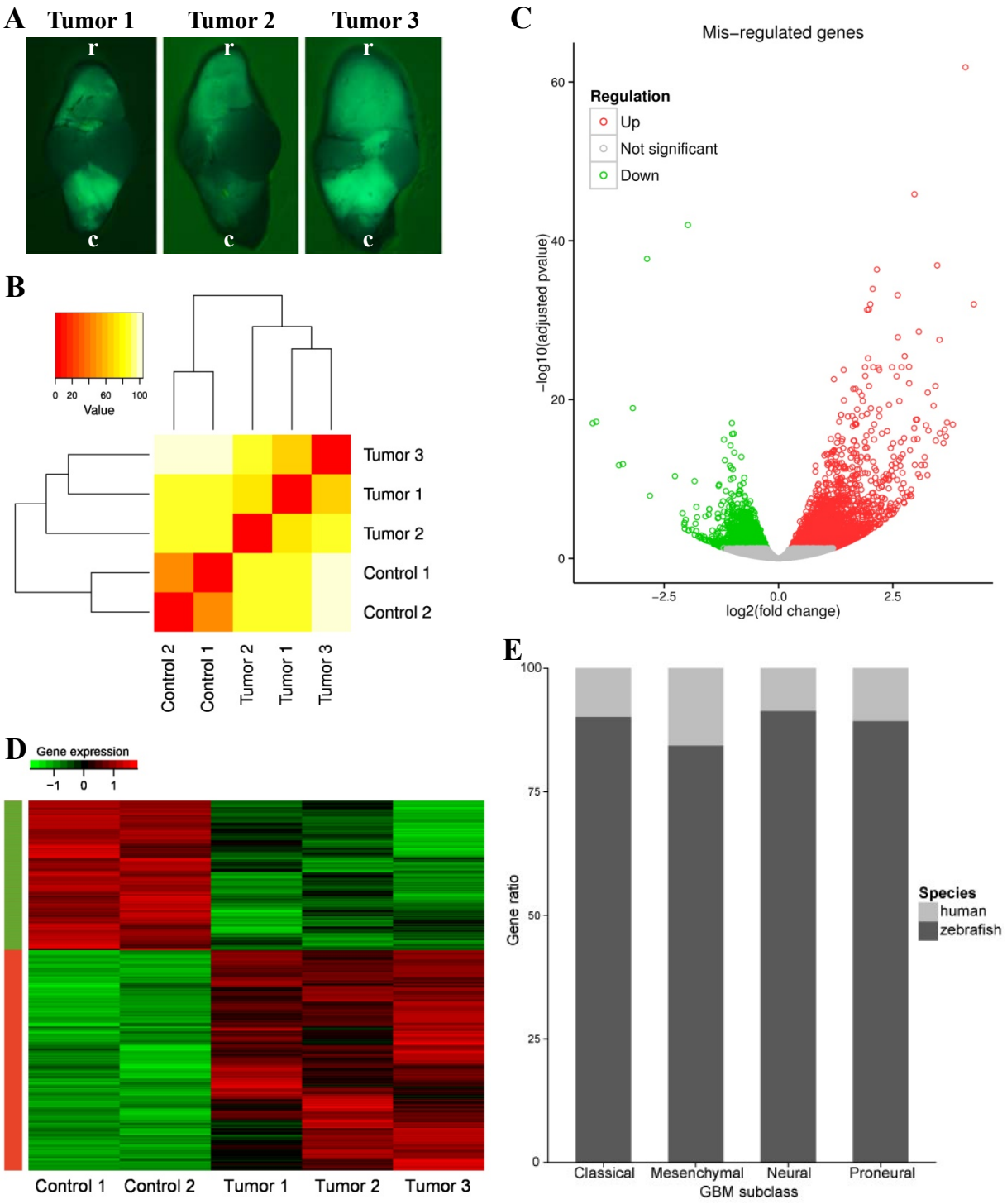

Figure S5: *Quality control for zebrafish model RNAseq results.*
A) Dorsal view of stereo images of whole brains from zic:$RAS_{somatic}$ used for RNAseq analysis (r=rostral, c=caudal). **B**) Hierarchical clustering of control and tumour samples using Euclidean distance on gene expression grouped the samples according to tumour or control. **C**) The volcano plot represents all known zebrafish genes for which a differential expression analysis was done. The significantly differentially expressed (DE) genes (adjusted p-value<0.05) are coloured in red (up-regulated) or green (down-regulated). **D**) After clustering of significantly (adjusted p-value<0.05) DE genes based on normalised expression, the genes clustered according to regulation, verifying the efficiency of the normalisation step. **E**) After the identification of the zebrafish orthologs of the 840 GBM human markers, through Ensembl annotation and manual refinement, more than 80 % of genes could be identified for all four GBM subclasses.

Figure S6

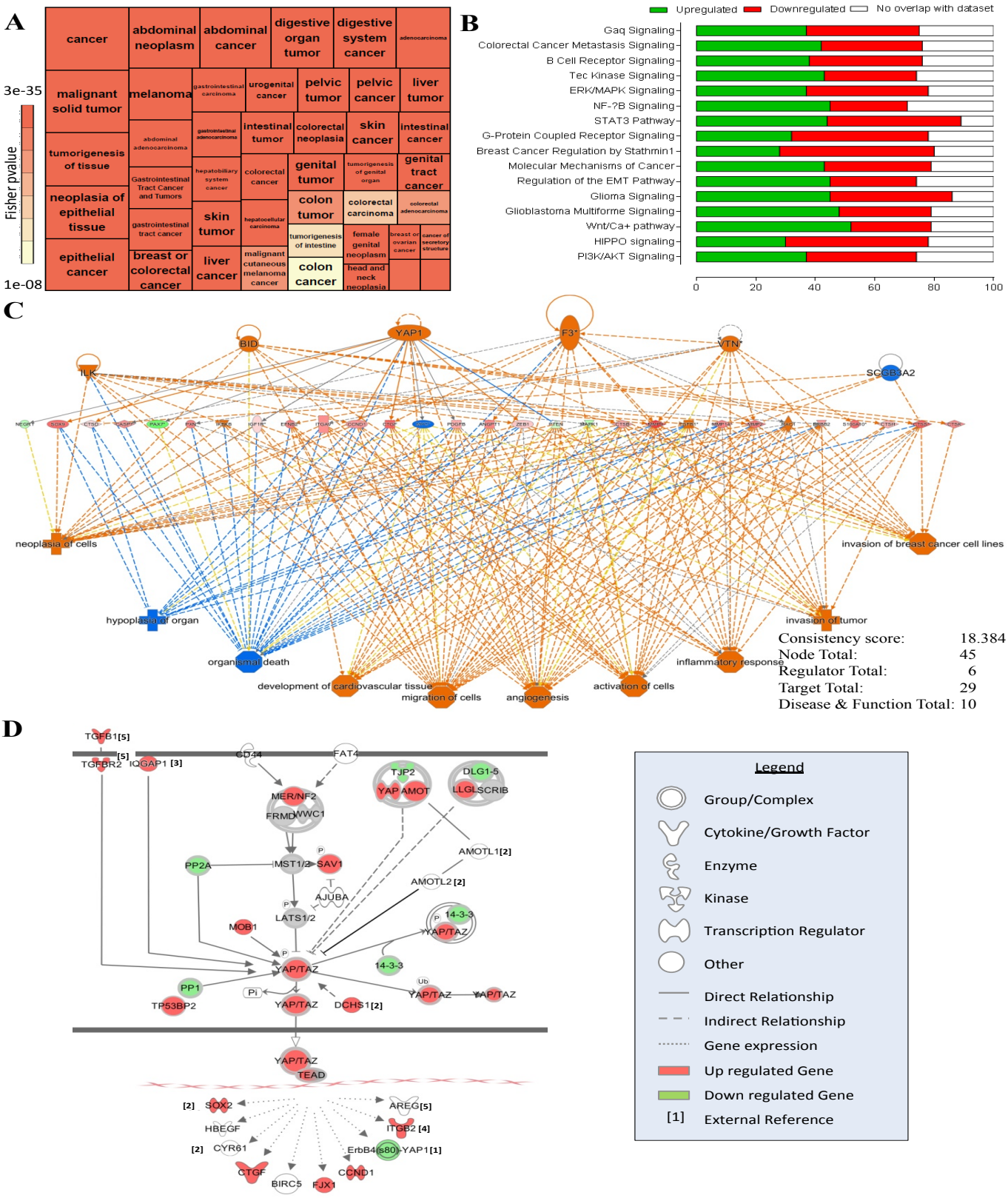

Figure S6: *IPA analysis highlights the oncogenic nature of the model and suggests YAP as a key regulator in this tumour model.*

A) The treemap represents IPA results for the disease significantly enriched and belonging to the superfamily "Cancer". The color scale fits to the significance (Fisher p-value) and the square size of the squares to the number of genes associated to each disease. **B**) Selection of cancer associated pathways determined by IPA to be highly significantly enriched (p-value<2E-06). **C**) The most consistent "Regulator Effects Network", that IPA generates by linking Upstream Regulators via their target genes to physiological effects, contains 6 Upstream Regulators with YAP appearing as the most interconnected Upstream Regulator. **D**) This YAP network has been based on IPA knowledge-base and more information were gathered through scientific literature. Key players, including YAP and TAZ, are found significantly (adjusted p-value<0.05) differentially expressed. The significantly upregulated genes are coloured in red and the downregulated genes in green. [1] = Mo et al., 2014; [2] = Kodaka et al., 2015; [3] = Anakk et al., 2013; [4] = Lim et al., 2014; [5] = Piccolo et al., 2014

A

Gene name	Log2-Fc	p-value
yap1	1.31	6.30E-06
ccnd1	1.15	9.49E-04
ctgfa	1.68	4.41E-22
iqgap1	1.95	1.90E-11
itgb2	1.11	4.39E-06
tgfb1a	1.56	4.85E-05
tgfbr2	1.15	5.12E-10
amot	1.43	1.22E-20
amotl2a	0.18	6.13E-01
amotl2b	0.44	4.31E-01
tp53bp2	0.73	9.02E-03
birc5a	-0.78	1.96E-01
wwtr1	0.77	4.20E-03
cyr61	0.47	5.22E-01
hbegfa	2.02	1.25E-19
hbegfb	0.87	4.53E-02
dlg4	-0.98	1.95E-16
erbb4a	-0.88	7.92E-09
sox2	1.05	2.74E-09
tjp2a	-0.69	2.08E-02
ywhag1	-0.63	3.12E-03
ywhah	-0.51	7.21E-03

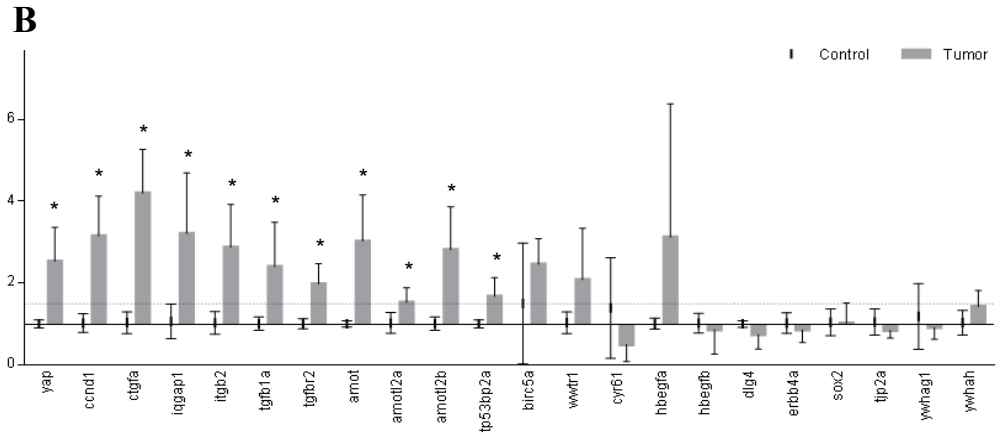

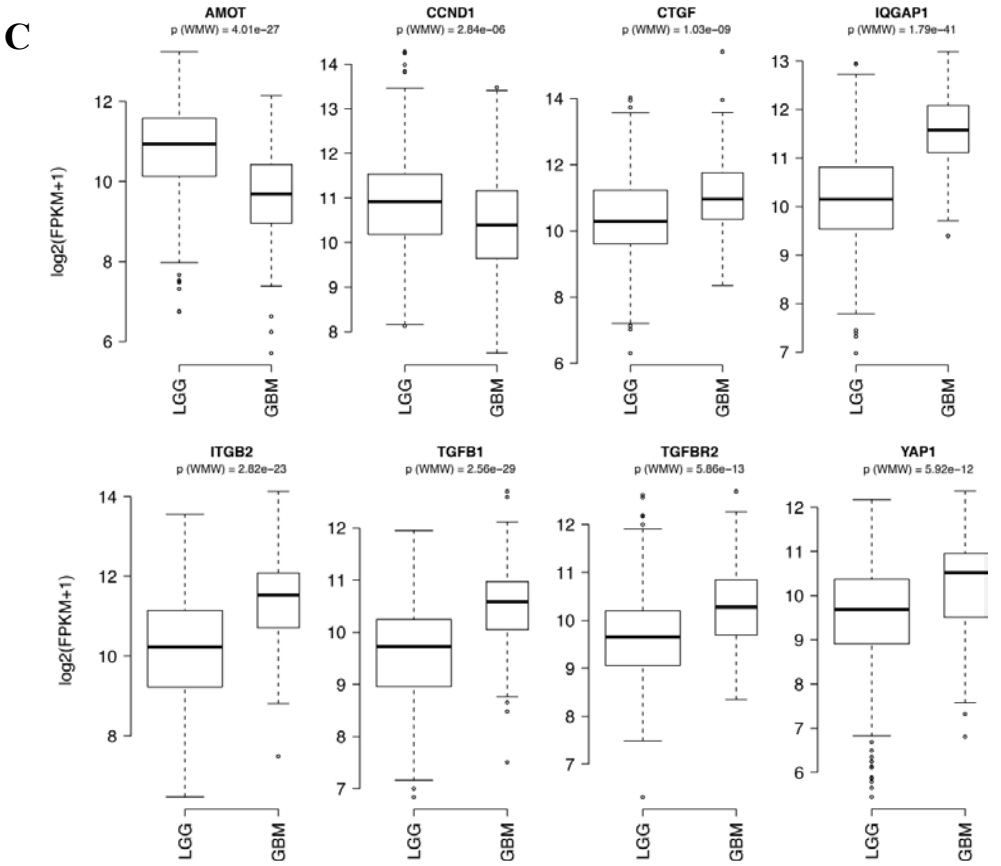

Figure S7: *YAP signature is enriched in the zebrafish glioma model.*
A) List of YAP related genes with their log2-fold change and p-value determined by RNAseq analysis of control brains (n=3) and tumours (n=3). **B**) Fold change of expression of YAP related genes determined by qPCR of control brains (n=3) and tumours (n=3). **C**) Box plots of the gene expression of the eigth signature genes in GBM (n = 166) and LGG (n = 530) TCGA samples. Reported p-values are estimated by wilcoxon mann whitney (WMW) test. Data are represented as mean ± SEM; *pvalue<0.05.

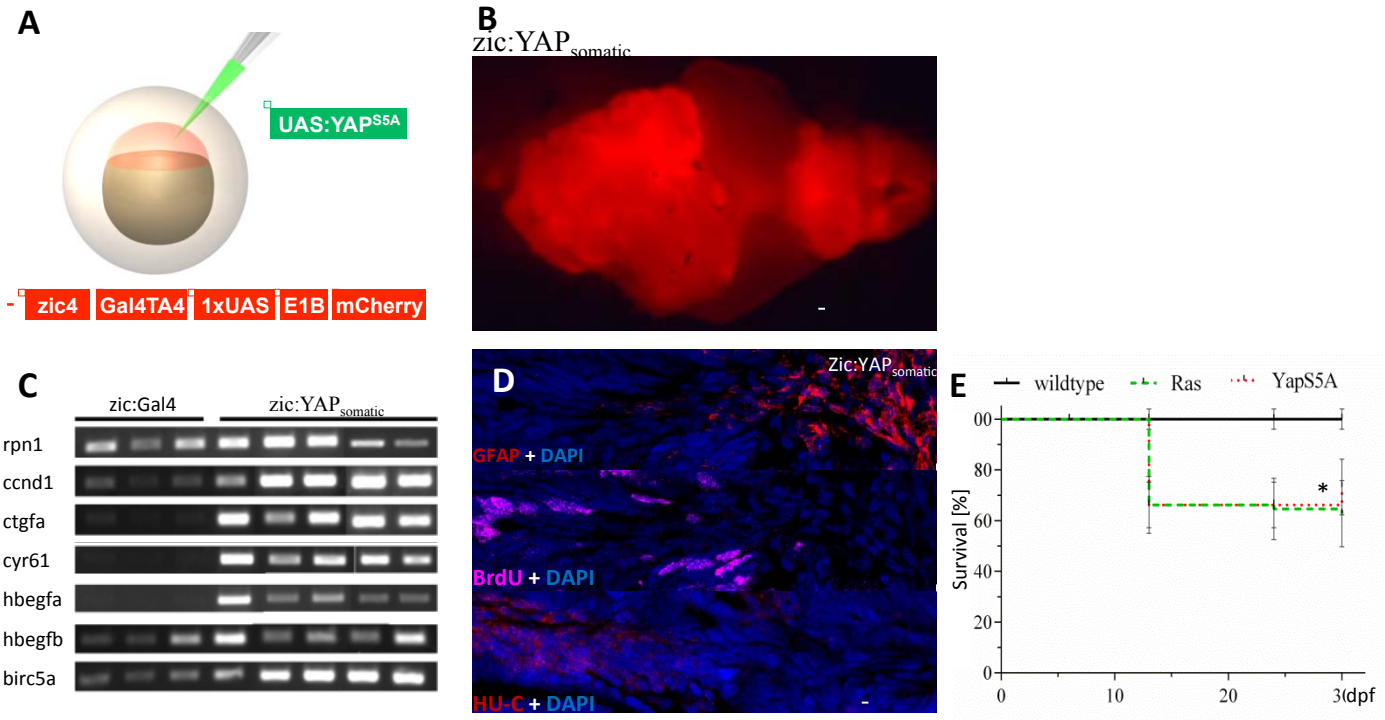

Figure S8: *Ectopic YAP expression induces brain tumour development.*
A) Schematic representation of tumour induction through the injection of oncogenic constructs (green) into zic:Gal4 embryos. **B**) Stereo image of a tumour developed in zic:$YAP_{somatic}$. **C**) YAP target gene expression in zic:Gal4 control brains and zic:$YAP_{somatic}$ tumours. **D**) Immunostaining for BrdU, GFAP and HU-C of zic:$YAP_{somatic}$ tumours. **E**) Survival rate of zic:$RAS_{somatic}$ (green dashed line) and zic:$YAP_{somatic}$ (red dotted line) compared to zic:Gal4 (black solid line, black asterix). Data are represented as mean ± SD. Scale bars: **B** = 2 mm; **G** = 20 µm; *p-value<0.05.

Table S1
List of oncogenes/transgenes used.

Name of construct	**Short name**	**References**
UAS:eGFP-HRAS_G12V	UAS:GFP-HRAS^{V12}	Santoriello et al., 2010
UAS:Hsa.HIST2H2BE-CFP,Hsa.HRAS_G12V	UAS:CFP-HRAS^{V12}	Alghisi et al., 2012
UAS:eGFP-KRAS_G12V	UAS:GFP-KRAS^{V12}	Park et al., 2014
UAS:BRAFV600E	UAS:BRAF^{E600}	This study
UAS:Xmrk	UAS:Xmrk	This study
UAS:myr-AKT-BFP	UAS:AKT-BFP	This study
UAS:eGFP-EGFRvIII	UAS:EGFR$_{VIII}$	This study
UAS:YAPS5A	UAS:YAP^{S5A}	This study
UAS:LifeAct-GFP	UAS:LA-GFP	This study

Table S2
List of all brains analized in this study. Oncogene= oncogene used, specifying whether through germline or somatic expression; Age = age of fish at the time of brain resection, Tel = telencephalic tumour, DD = dorsal diencephalic tumour, IVth ventr = IVth ventricular tumour, Het = heterotopia.

Brain	Oncogene (germline)	Age [days]	Image	Tel	DD	IV Ventr
1	UAS:GFP-HRAS^{V12}	69	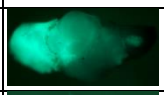	yes	yes	yes
2	UAS:GFP-HRAS^{V12}	39	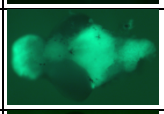	yes	yes	yes
3	UAS:GFP-HRAS^{V12}	39	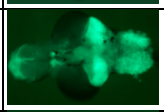	yes	yes	yes
4	UAS:GFP-HRAS^{V12}	30	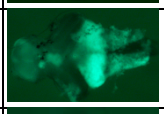	yes	yes	yes
5	UAS:GFP-HRAS^{V12}	30	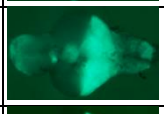	yes	yes	yes
6	UAS:GFP-HRAS^{V12}	30	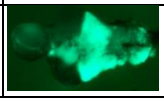	yes	yes	yes

7	UAS:GFP-HRAS^{V12}	30	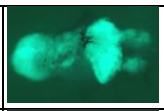	yes	yes	yes
8	UAS:GFP-HRAS^{V12}	39	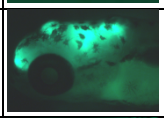	yes	yes	yes
9	UAS:GFP-HRAS^{V12}	39	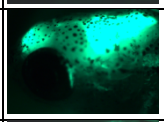	yes	yes	yes
10	UAS:GFP-HRAS^{V12}	39	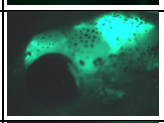	yes	yes	yes
11	UAS:GFP-HRAS^{V12}	39	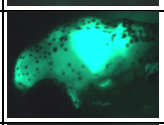	yes	yes	yes
12	UAS:GFP-HRAS^{V12}	39	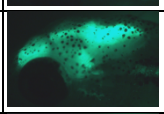	yes	yes	yes
13	UAS:GFP-HRAS^{V12}	39	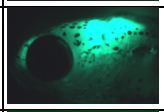	yes	yes	yes
14	UAS:GFP-HRAS^{V12}	56	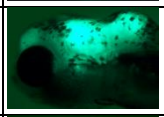	yes	yes	yes
15	UAS:GFP-HRAS^{V12}	59	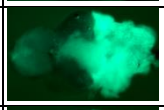	yes	yes	yes
16	UAS:GFP-HRAS^{V12}	59	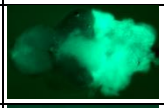	yes	yes	yes
17	UAS:GFP-HRAS^{V12}	59	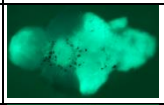	yes	yes	yes
18	UAS:GFP-HRAS^{V12}	59	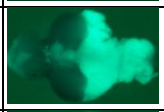	yes	yes	yes
19	UAS:GFP-HRAS^{V12}	113	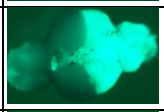	yes	yes	yes
20	UAS:GFP-HRAS^{V12}	113		yes	yes	yes
21	UAS:GFP-HRAS^{V12}	113		no	yes	yes
22	UAS:GFP-HRAS^{V12}	113	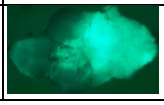	yes	yes	yes

23	UAS:GFP-HRAS^{V12}	113	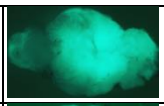	yes	yes	yes
24	UAS:GFP-HRAS^{V12}	113	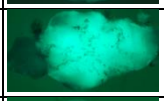	no	yes	yes
25	UAS:GFP-HRAS^{V12}	113	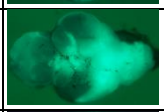	yes	yes	yes
26	UAS:GFP-HRAS^{V12}	73	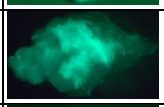	yes	yes	yes
27	UAS:GFP-HRAS^{V12}	114		yes	yes	yes
28	UAS:GFP-HRAS^{V12}	73		yes	yes	yes
29	UAS:GFP-HRAS^{V12}	114	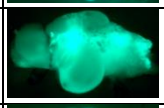	yes	yes	yes
30	UAS:GFP-HRAS^{V12}	114	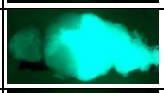	yes	yes	yes
31	UAS:GFP-HRAS^{V12}	138	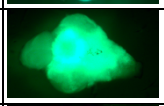	yes	yes	yes
32	UAS:GFP-HRAS^{V12}	224	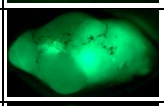	yes	yes	yes
33	UAS:GFP-HRAS^{V12}	224	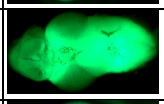	yes	yes	yes
34	UAS:GFP-HRAS^{V12}	224	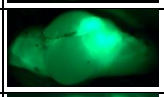	yes	yes	yes
35	UAS:GFP-HRAS^{V12}	227	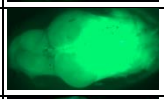	yes	yes	yes
36	UAS:GFP-HRAS^{V12}	119	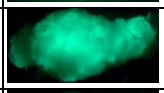	yes	yes	yes
37	UAS:GFP-HRAS^{V12}	119	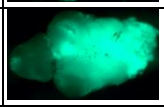	yes	yes	yes
38	UAS:GFP-HRAS^{V12}	119	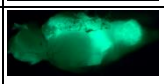	yes	yes	yes
39	UAS:GFP-HRAS^{V12}	119	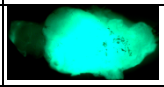	yes	yes	yes
40	UAS:GFP-HRAS^{V12}	119	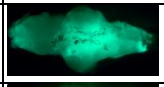	yes	yes	yes
41	UAS:GFP-HRAS^{V12}	175	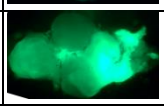	yes	yes	yes

42	UAS:GFP-HRAS^{V12}	175	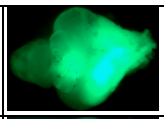	yes	yes	yes	
43	UAS:GFP-HRAS^{V12}	175	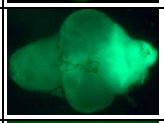	yes	yes	yes	
44	UAS:GFP-HRAS^{V12}	39		yes	yes	yes	
45	UAS:GFP-HRAS^{V12}	39	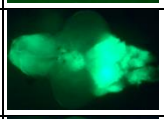	yes	yes	yes	
46	UAS:GFP-HRAS^{V12}	94	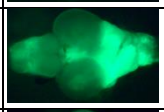	yes	yes	yes	
47	UAS:GFP-HRAS^{V12}	94	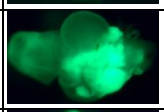	yes	yes	yes	
48	UAS:GFP-HRAS^{V12}	123	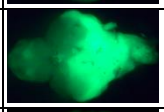	yes	yes	yes	
49	UAS:GFP-HRAS^{V12}	123	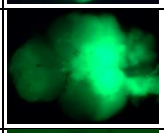	yes	yes	yes	
50	UAS:GFP-HRAS^{V12}	39	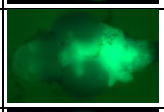	yes	yes	yes	
51	UAS:GFP-HRAS^{V12}	39	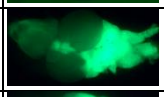	yes	yes	yes	
52	UAS:GFP-HRAS^{V12}	95	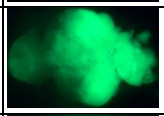	yes	yes	yes	
53	UAS:GFP-HRAS^{V12}	95	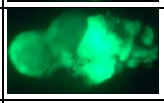	yes	yes	yes	

brain	Oncogene (somatic)	Age [days]	Image	Tel	DD	IV Ventr	Het.
1	UAS:GFP-HRAS^{V12}	69		no	no	no	yes
2	UAS:GFP-HRAS^{V12}	69		yes	yes	no	yes
3	UAS:GFP-HRAS^{V12}	62		no	no	no	yes
4	UAS:GFP-HRAS^{V12}	62	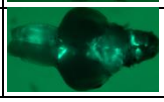	no	no	yes	yes

5	UAS:GFP-HRAS^{V12}	75	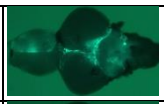	no	no	no	no
6	UAS:GFP-HRAS^{V12}	75	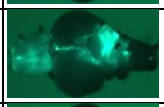	no	no	no	yes
7	UAS:GFP-HRAS^{V12}	75	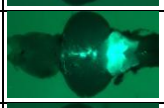	no	no	no	yes
8	UAS:GFP-HRAS^{V12}	75		yes	no	no	no
9	UAS:GFP-HRAS^{V12}	49		yes	yes	yes	yes
10	UAS:GFP-HRAS^{V12}	33	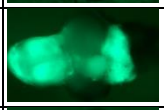	yes	yes	yes	no
11	UAS:GFP-HRAS^{V12}	33	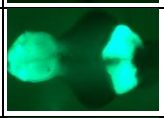	yes	no	yes	no
12	UAS:GFP-HRAS^{V12}	33	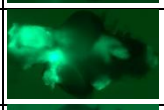	yes	yes	no	yes
13	UAS:GFP-HRAS^{V12}	33	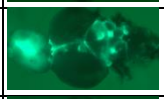	yes	no	no	yes
14	UAS:GFP-HRAS^{V12}	33		yes	no	yes	yes
15	UAS:GFP-HRAS^{V12}	69	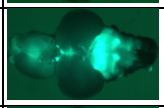	no	no	no	no
16	UAS:GFP-HRAS^{V12}	69	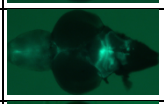	no	no	no	no
17	UAS:GFP-HRAS^{V12}	69		no	no	no	no
18	UAS:GFP-HRAS^{V12}	40	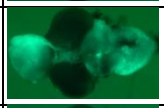	yes	yes	yes	yes
19	UAS:GFP-HRAS^{V12}	40	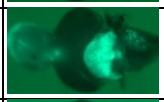	yes	no	yes	no
20	UAS:GFP-HRAS^{V12}	40	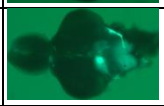	no	no	no	yes
21	UAS:GFP-HRAS^{V12}	40		yes	no	yes	yes
22	UAS:GFP-HRAS^{V12}	40	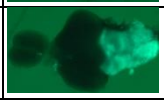	no	no	yes	yes

23	UAS:GFP-HRAS^{V12}	67	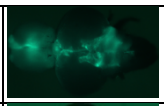	no	no	no	yes
24	UAS:GFP-HRAS^{V12}	67		no	no	no	yes
25	UAS:GFP-HRAS^{V12}	67	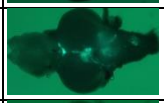	no	no	no	no
26	UAS:GFP-HRAS^{V12}	44		yes	no	no	no
27	UAS:GFP-HRAS^{V12}	44		no	no	no	no
28	UAS:GFP-HRAS^{V12}	44		no	no	no	yes
29	UAS:GFP-HRAS^{V12}	44		yes	no	no	no
30	UAS:GFP-HRAS^{V12}	44		yes	no	no	yes
31	UAS:GFP-HRAS^{V12}	44		no	no	no	no
32	UAS:GFP-HRAS^{V12}	44	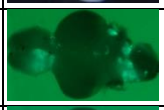	no	no	no	yes
33	UAS:GFP-HRAS^{V12}	44		no	no	no	yes
34	UAS:GFP-HRAS^{V12}	44		yes	no	no	no
35	UAS:GFP-HRAS^{V12}	44		no	no	yes	yes
36	UAS:GFP-HRAS^{V12}	44		no	no	yes	no
37	UAS:GFP-HRAS^{V12}	61		yes	yes	no	yes
38	UAS:GFP-HRAS^{V12}	61	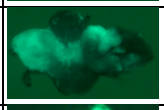	yes	yes	yes	yes
39	UAS:GFP-HRAS^{V12}	55	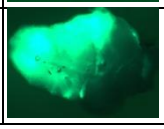	yes	yes	no	no

40	UAS:GFP-HRAS^{V12}	112	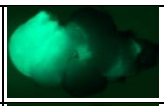	yes	yes	no	yes
41	UAS:GFP-HRAS^{V12}	57	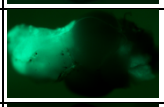	yes	no	no	yes
42	UAS:GFP-HRAS^{V12}	57	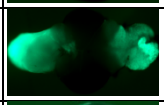	yes	no	yes	yes
43	UAS:GFP-HRAS^{V12}	57		yes	yes	no	yes
44	UAS:GFP-HRAS^{V12}	57	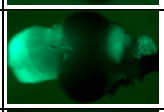	yes	no	yes	yes
45	UAS:GFP-HRAS^{V12}	79	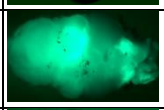	yes	yes	yes	yes
46	UAS:GFP-HRAS^{V12}	153		yes	no	no	no
47	UAS:GFP-HRAS^{V12}	128	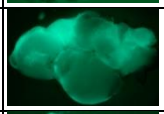	yes	no	yes	yes
48	UAS:GFP-HRAS^{V12}	128	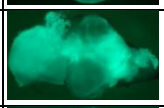	yes	yes	yes	yes
49	UAS:GFP-HRAS^{V12}	128		yes	yes	yes	yes
50	UAS:GFP-HRAS^{V12}	128	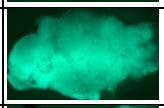	yes	yes	yes	yes
51	UAS:GFP-HRAS^{V12}	128		no	no	yes	yes
52	UAS:GFP-HRAS^{V12}	14	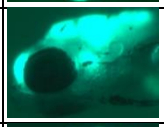	yes	yes	yes	yes
53	UAS:GFP-HRAS^{V12}	14		yes	no	yes	yes
54	UAS:GFP-HRAS^{V12}	26	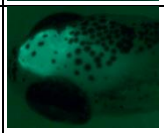	yes	no	no	no
55	UAS:GFP-HRAS^{V12}	132	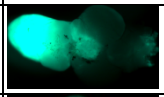	yes	yes	no	yes
56	UAS:GFP-HRAS^{V12}	132	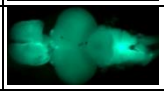	no	no	no	yes

57	UAS:GFP-HRAS^{V12}	135	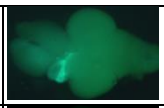	no	no	no	yes
58	UAS:GFP-HRAS^{V12}	408	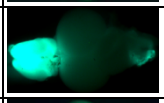	yes	no	no	no
59	UAS:GFP-HRAS^{V12}	143	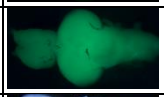	no	no	no	no
60	UAS:GFP-HRAS^{V12}	254		no	no	no	no
61	UAS:GFP-HRAS^{V12}	21	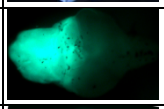	yes	no	no	no
62	UAS:GFP-HRAS^{V12}	61	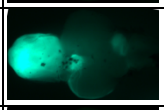	yes	yes	no	no
63	UAS:GFP-HRAS^{V12}	149	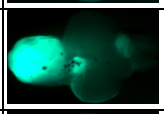	no	no	no	yes
64	UAS:GFP-HRAS^{V12}	90	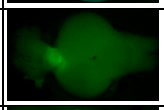	no	no	no	yes
65	UAS:GFP-HRAS^{V12}	49	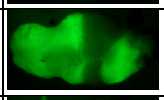	yes	yes	yes	no
66	UAS:GFP-HRAS^{V12}	49	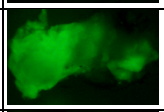	yes	yes	yes	no
67	UAS:GFP-HRAS^{V12}	49	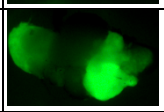	yes	no	yes	no
68	UAS:GFP-HRAS^{V12}	179	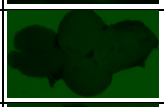	no	no	no	no
69	UAS:GFP-HRAS^{V12}	179	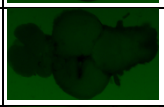	no	no	no	yes
70	UAS:GFP-HRAS^{V12}	61	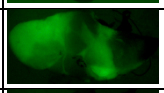	yes	no	yes	no
71	UAS:GFP-HRAS^{V12}	61	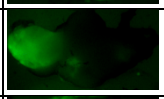	yes	yes	no	yes
72	UAS:GFP-HRAS^{V12}	61	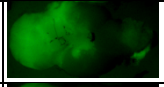	yes	yes	no	no
73	UAS:GFP-HRAS^{V12}	61	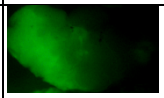	yes	yes	no	no
74	UAS:GFP-HRAS^{V12}	61	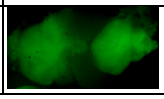	yes	yes	yes	yes

75	UAS:GFP-HRAS^{V12}	111	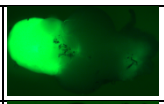	yes	no	no	no
76	UAS:GFP-HRAS^{V12}	311	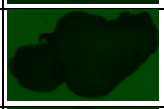	no	no	no	no
77	UAS:GFP-HRAS^{V12}	311	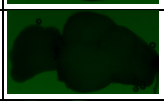	no	no	no	no
78	UAS:GFP-HRAS^{V12}	177	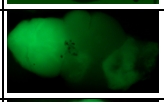	yes	no	yes	yes
79	UAS:GFP-HRAS^{V12}	177	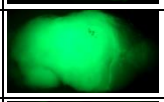	yes	yes	no	no
80	UAS:GFP-HRAS^{V12}	70	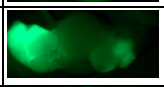	yes	no	yes	no
81	UAS:GFP-HRAS^{V12}	70	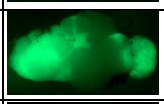	yes	yes	yes	yes
82	UAS:GFP-HRAS^{V12}	440	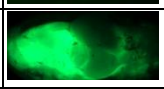	yes	no	no	yes
83	UAS:GFP-HRAS^{V12}	440	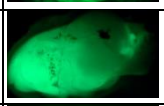	yes	no	yes	no
84	UAS:GFP-HRAS^{V12}	106	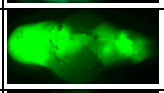	yes	yes	yes	yes
85	UAS:GFP-HRAS^{V12}	106	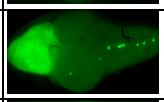	yes	no	no	no
86	UAS:GFP-HRAS^{V12}	106	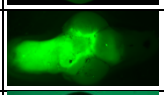	yes	yes	no	no
87	UAS:GFP-HRAS^{V12}	37	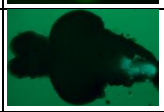	no	no	no	no
88	UAS:GFP-HRAS^{V12}	37	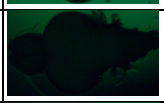	no	no	no	no
89	UAS:GFP-HRAS^{V12}	37		no	no	no	yes
90	UAS:GFP-HRAS^{V12}	37	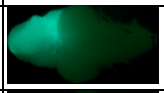	yes	no	no	no
91	UAS:GFP-HRAS^{V12}	37	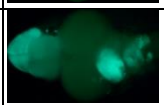	yes	no	yes	no
92	UAS:GFP-HRAS^{V12}	37	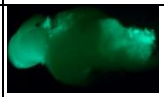	yes	no	yes	no
93	UAS:GFP-HRAS^{V12}	37	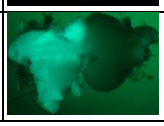	yes	no	no	no

94	UAS:GFP-HRAS^{V12}	37	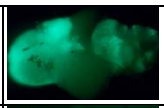	yes	yes	yes	no
95	UAS:GFP-HRAS^{V12}	37	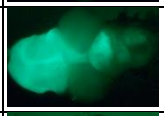	yes	no	yes	no
96	UAS:GFP-HRAS^{V12}	37		yes	yes	yes	no
97	UAS:GFP-HRAS^{V12}	37		no	no	no	no
98	UAS:GFP-HRAS^{V12}	37	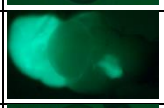	yes	no	no	no
99	UAS:GFP-HRAS^{V12}	37		no	no	no	no
100	UAS:GFP-HRAS^{V12}	37	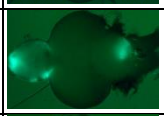	no	no	no	no
101	UAS:GFP-HRAS^{V12}	37	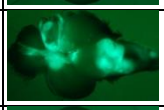	no	yes	yes	yes
102	UAS:GFP-HRAS^{V12}	37		no	no	yes	no
103	UAS:GFP-HRAS^{V12}	37	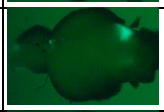	no	no	no	no
104	UAS:GFP-HRAS^{V12}	37		no	no	no	no
105	UAS:GFP-HRAS^{V12}	37		no	no	no	no
106	UAS:GFP-HRAS^{V12}	37		no	no	no	no
107	UAS:GFP-HRAS^{V12}	37		no	no	no	no
108	UAS:GFP-HRAS^{V12}	37	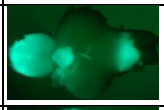	yes	yes	yes	yes
109	UAS:GFP-HRAS^{V12}	37	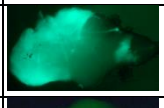	yes	yes	no	no
110	UAS:GFP-HRAS^{V12}	37	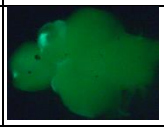	no	no	no	yes

111	UAS:GFP-HRAS^{V12}	37	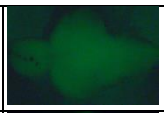	no	no	no	no
112	UAS:GFP-HRAS^{V12}	37	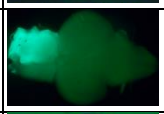	yes	no	no	no
113	UAS:GFP-HRAS^{V12}	264		yes	yes	no	no
114	UAS:GFP-HRAS^{V12}	122		yes	yes	yes	yes
115	UAS:GFP-HRAS^{V12}	122		yes	yes	yes	yes
116	UAS:GFP-HRAS^{V12}	122	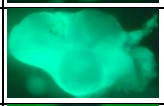	yes	yes	yes	yes
117	UAS:GFP-HRAS^{V12}	609	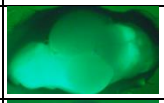	yes	no	no	no
118	UAS:GFP-HRAS^{V12}	609	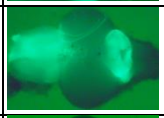	yes	no	yes	no
119	UAS:GFP-HRAS^{V12}	609	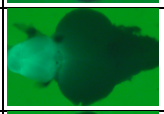	yes	no	no	no
120	UAS:GFP-HRAS^{V12}	475		yes	no	yes	yes
121	UAS:GFP-HRAS^{V12}	475	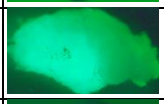	yes	no	no	no
122	UAS:GFP-HRAS^{V12}	145		yes	yes	no	no
123	UAS:GFP-HRAS^{V12}	145	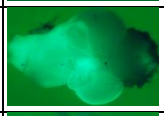	yes	yes	no	yes
124	UAS:GFP-HRAS^{V12}	145		yes	no	no	yes
125	UAS:GFP-HRAS^{V12}	145	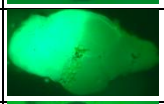	yes	no	no	yes
126	UAS:GFP-HRAS^{V12}	145	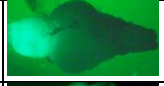	yes	no	no	no
127	UAS:GFP-HRAS^{V12}	259	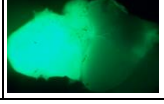	yes	yes	no	yes

128	UAS:GFP-HRAS^{V12}	259	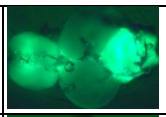	no	no	yes	yes
129	UAS:GFP-HRAS^{V12}	33	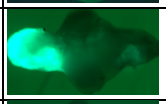	yes	no	no	Yes
130	UAS:GFP-HRAS^{V12}	33	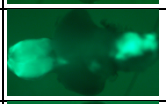	yes	no	yes	yes
131	UAS:GFP-HRAS^{V12}	33	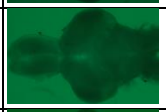	no	no	no	yes
132	UAS:GFP-HRAS^{V12}	33	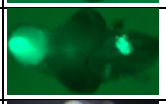	yes	no	yes	yes
133	UAS:GFP-HRAS^{V12}	33	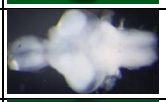	no	no	no	yes
134	UAS:GFP-HRAS^{V12}	33		yes	yes	no	yes
135	UAS:GFP-KRAS^{V12}	25	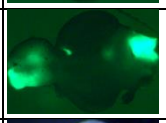	yes	no	yes	yes
136	UAS:GFP-KRAS^{V12}	25	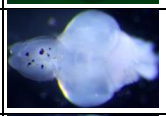	no	no	no	no
137	UAS:GFP-KRAS^{V12}	25	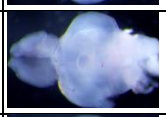	no	no	no	no
138	UAS:GFP-KRAS^{V12}	25		no	no	no	yes
139	UAS:GFP-KRAS^{V12}	27		no	no	yes	yes
140	UAS:GFP-KRAS^{V12}	27	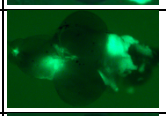	yes	no	yes	yes
141	UAS:GFP-KRAS^{V12}	27	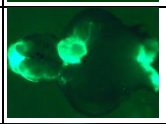	yes	yes	yes	yes
142	UAS:GFP-KRAS^{V12}	27	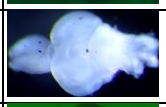	no	no	no	no
143	UAS:GFP-KRAS^{V12}	27	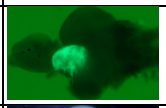	no	yes	no	yes
144	UAS:GFP-KRAS^{V12}	27	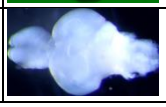	no	no	no	no

145	UAS:GFP-KRAS^{V12}	47	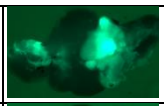	yes	no	yes	yes
146	UAS:GFP-KRAS^{V12}	47	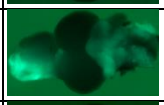	yes	no	yes	yes
147	UAS:GFP-KRAS^{V12}	47	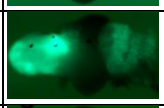	yes	no	yes	yes
148	UAS:GFP-KRAS^{V12}	47	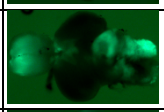	yes	yes	yes	no
149	UAS:GFP-KRAS^{V12}	47	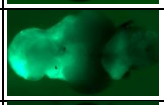	yes	yes	yes	no
150	UAS:GFP-KRAS^{V12}	47		no	no	no	no
151	UAS:GFP-KRAS^{V12}	170	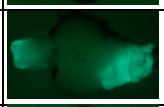	no	no	yes	no
152	UAS:GFP-KRAS^{V12}	170		no	no	no	no
153	UAS:GFP-KRAS^{V12}	170	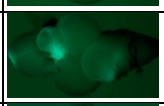	no	no	no	yes
154	UAS:GFP-KRAS^{V12}	170	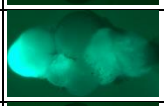	yes	yes	yes	yes
155	UAS:GFP-KRAS^{V12}	210	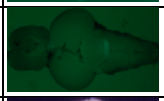	no	no	no	no
156	UAS:CFP-HRAS^{V12}	408		no	no	no	yes
157	UAS:CFP-HRAS^{V12}	169		no	no	no	yes
158	UAS:CFP-HRAS^{V12}	169		no	no	no	yes
159	UAS:CFP-HRAS^{V12}	41	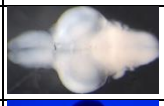	no	no	no	yes
160	UAS:CFP-HRAS^{V12}	34	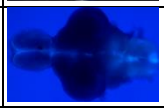	no	no	yes	yes
161	UAS:CFP-HRAS^{V12}	34		no	no	no	yes
162	UAS:CFP-HRAS^{V12}	34		no	no	no	yes

163	UAS:CFP-HRAS^{V12}	44		no	no	yes	no
164	UAS:CFP-HRAS^{V12}	50		no	no	yes	yes
165	UAS:CFP-HRAS^{V12}	50		no	no	yes	yes
166	UAS:CFP-HRAS^{V12}	50		no	no	yes	yes
167	UAS:CFP-HRAS^{V12}	50		no	no	yes	yes
168	UAS:CFP-HRAS^{V12}	50		no	no	yes	yes
169	UAS:CFP-HRAS^{V12}	50	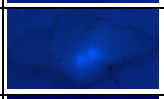	no	yes	yes	yes
170	UAS:CFP-HRAS^{V12}	50	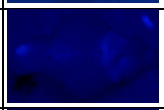	no	yes	yes	yes
171	UAS:CFP-HRAS^{V12}	48	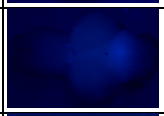	no	no	yes	no
172	UAS:CFP-HRAS^{V12}	48		no	no	yes	yes
173	UAS:CFP-HRAS^{V12}	48		no	no	yes	no
174	UAS:CFP-HRAS^{V12}	48	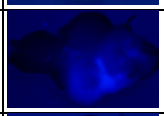	no	yes	yes	yes
175	UAS:CFP-HRAS^{V12}	48	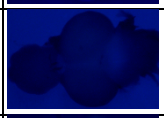	no	no	no	yes
176	UAS:CFP-HRAS^{V12}	48		no	no	no	yes
177	UAS:CFP-HRAS^{V12}	48	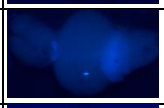	no	no	yes	yes
178	UAS:CFP-HRAS^{V12}	48	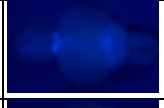	no	no	yes	no
179	UAS:CFP-HRAS^{V12}	48	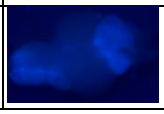	yes	yes	yes	yes

180	UAS:CFP-HRAS^{V12}	48	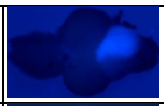	no	no	yes	yes
181	UAS:CFP-HRAS^{V12}	135		no	no	yes	yes
182	UAS:CFP-HRAS^{V12}	256	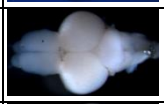	no	no	no	no
183	UAS:CFP-HRAS^{V12}	256		no	no	no	yes
184	UAS:CFP-HRAS^{V12}	260	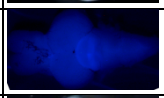	no	no	yes	yes
185	UAS:CFP-HRAS^{V12}	254		no	no	no	no
186	UAS:CFP-HRAS^{V12}	283		no	no	no	no
187	UAS:CFP-HRAS^{V12}	283		no	no	no	yes
188	UAS:CFP-HRAS^{V12}	283		no	no	no	no
189	UAS:CFP-HRAS^{V12}	283		no	no	no	yes
190	UAS:CFP-HRAS^{V12}	283	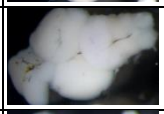	no	no	no	yes
191	UAS:EGFR$_{VIII}$	79	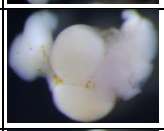	no	no	no	yes
192	UAS:EGFR$_{VIII}$	79		no	no	no	no
193	UAS:EGFR$_{VIII}$	79	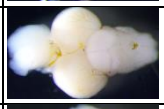	no	no	no	no
194	UAS:EGFR$_{VIII}$	79	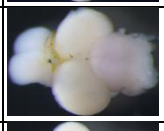	no	no	no	no
195	UAS:EGFR$_{VIII}$	79	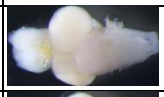	no	no	no	no
196	UAS:EGFR$_{VIII}$	79		no	no	no	no

197	UAS:AKT-BFP	26	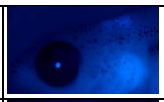	no	no	yes	no
198	UAS:AKT-BFP	62		yes	no	yes	no
199	UAS:AKT-BFP	62	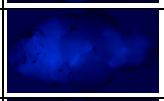	yes	yes	yes	yes
200	UAS:AKT-BFP	34	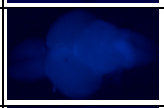	no	no	yes	yes
201	UAS:AKT-BFP	34		yes	no	yes	yes
202	UAS:AKT-BFP	42075		no	no	yes	no
203	UAS:AKT-BFP	42075		no	no	yes	no
204	UAS:AKT-BFP	42075		no	no	yes	yes
205	UAS:AKT-BFP	279	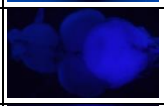	no	no	yes	no
206	UAS:AKT-BFP	340	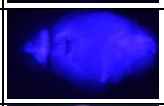	yes	yes	yes	no
207	UAS:AKT-BFP	340		no	no	no	no
208	UAS:AKT-BFP	340		no	no	no	no
209	UAS:AKT-BFP	340		no	no	no	no
210	UAS:AKT-BFP	340		no	no	no	no
211	UAS:AKT-BFP	340		no	no	no	no
212	UAS:AKT-BFP	320	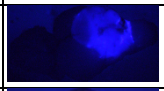	no	no	yes	no
213	UAS:AKT-BFP	320		no	no	yes	no
214	UAS:AKT-BFP	280	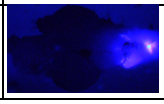	no	no	yes	no

215	UAS:AKT-BFP	421		no	no	no	yes
216	UAS:AKT-BFP + UAS:GFP-HRAS^{V12}	26	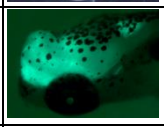	yes	yes	no	no
217	UAS:AKT-BFP + UAS:GFP-HRAS^{V12}	26	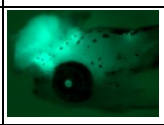	yes	no	no	no
218	UAS:AKT-BFP + UAS:GFP-HRAS^{V12}	36	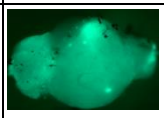	yes	yes	yes	no
219	UAS:AKT-BFP + UAS:GFP-HRAS^{V12}	60	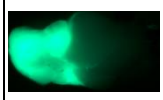	yes	no	no	no
220	UAS:AKT-BFP + UAS:GFP-HRAS^{V12}	60	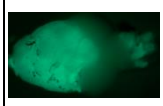	yes	yes	no	no
221	UAS:AKT-BFP + UAS:GFP-HRAS^{V12}	60	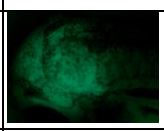	yes	yes	no	no
222	UAS:AKT-BFP + UAS:GFP-HRAS^{V12}	60	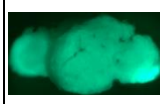	yes	yes	yes	no
223	UAS:AKT-BFP + UAS:GFP-HRAS^{V12}	98	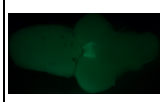	no	no	no	no
224	UAS:AKT-BFP + UAS:GFP-HRAS^{V12}	98	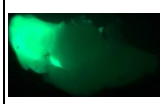	yes	no	no	no
225	UAS:AKT-BFP + UAS:GFP-HRAS^{V12}	179	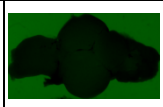	no	no	no	yes
226	UAS:AKT-BFP + UAS:GFP-HRAS^{V12}	179		no	no	yes	no
227	UAS:AKT-BFP + UAS:GFP-HRAS^{V12}	179	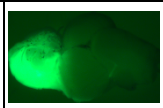	yes	no	no	no
228	UAS:AKT-BFP + UAS:GFP-HRAS^{V12}	70	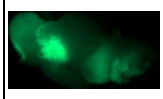	no	yes	no	yes
229	UAS:AKT-BFP + UAS:GFP-	70	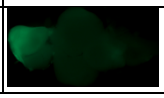	no	no	no	yes

	$HRAS^{V12}$						
230	UAS:AKT-BFP + UAS:GFP-$HRAS^{V12}$	70	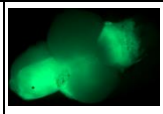	yes	yes	yes	no
231	UAS:AKT-BFP + UAS:GFP-$HRAS^{V12}$	58	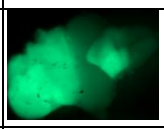	yes	no	yes	no
232	UAS:AKT-BFP + UAS:GFP-$HRAS^{V12}$	58	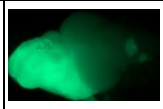	yes	no	no	yes
233	UAS:AKT-BFP + UAS:GFP-$HRAS^{V12}$	58	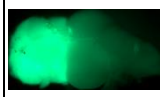	yes	no	no	no
234	UAS:AKT-BFP + UAS:GFP-$HRAS^{V12}$	58	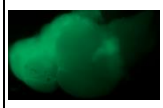	yes	no	no	no
235	UAS:AKT-BFP + UAS:GFP-$HRAS^{V12}$	72	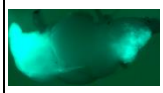	yes	no	yes	no
236	UAS:$BRAF^{E600}$ + UAS:LA-GFP	25		no	no	no	no
237	UAS:$BRAF^{E600}$ + UAS:LA-GFP	25		no	no	no	no
238	UAS:$BRAF^{E600}$ + UAS:LA-GFP	25	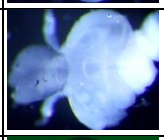	no	no	no	yes
239	UAS:$BRAF^{E600}$ + UAS:LA-GFP	25		no	no	yes	no
240	UAS:$BRAF^{E600}$ + UAS:LA-GFP	25		no	no	no	no
241	UAS:$BRAF^{E600}$ + UAS:LA-GFP	25	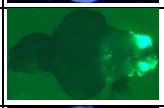	no	no	yes	yes
242	UAS:$BRAF^{E600}$ + UAS:LA-GFP	25		no	no	no	yes
243	UAS:$BRAF^{E600}$ + UAS:LA-GFP	85	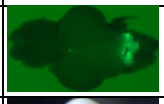	no	no	no	yes
244	UAS:$BRAF^{E600}$ + UAS:LA-GFP	85	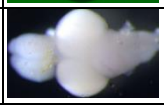	no	no	no	no

245	UAS:BRAF^{E600} + UAS:LA-GFP	85	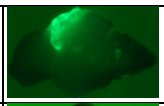	no	yes	no	yes
246	UAS:BRAF^{E600} + UAS:LA-GFP	85	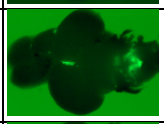	no	no	no	yes
247	UAS:BRAF^{E600} + UAS:LA-GFP	85	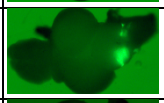	no	no	yes	yes
248	UAS:BRAF^{E600} + UAS:LA-GFP	85	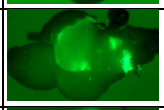	no	yes	yes	yes
249	UAS:BRAF^{E600} + UAS:LA-GFP	85	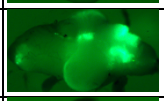	no	yes	yes	yes
250	UAS:BRAF^{E600} + UAS:LA-GFP	85	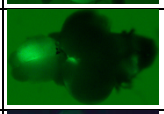	yes	no	no	yes
251	UAS:Xmrk + UAS:GFP	27	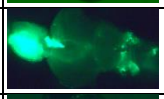	yes	no	no	no
252	UAS:Xmrk + UAS:GFP	27		no	no	yes	no
253	UAS:Xmrk + UAS:GFP	27		no	no	no	yes
254	UAS:Xmrk + UAS:GFP	27	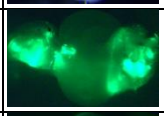	yes	no	yes	no
255	UAS:Xmrk + UAS:GFP	27	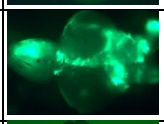	yes	no	yes	yes
256	UAS:Xmrk + UAS:GFP	77	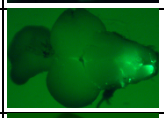	no	no	no	no
257	UAS:Xmrk + UAS:GFP	77	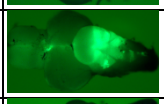	no	no	yes	no
258	UAS:Xmrk + UAS:GFP	77	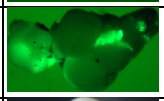	yes	no	no	no
259	UAS:Xmrk + UAS:GFP	77		no	no	no	no
260	UAS:GFP-HRAS^{V12} + UAS:Yap^{S5A}	39	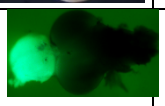	yes	no	no	no
261	UAS:GFP-HRAS^{V12} + UAS:Yap^{S5A}	39	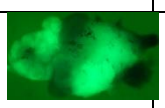	yes	no	yes	yes

262	UAS:GFP-HRAS^{V12} + UAS:Yap^{S5A}	21	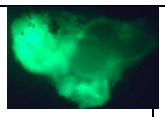	yes	yes	no	no
263	UAS:GFP-HRAS^{V12} + UAS:Yap^{S5A}	22	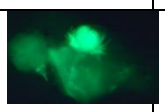	yes	yes	no	no
264	UAS:GFP-HRAS^{V12} + UAS:Yap^{S5A}	23	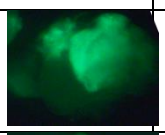	no	yes	yes	no
265	UAS:GFP-HRAS^{V12} + UAS:Yap^{S5A}	40	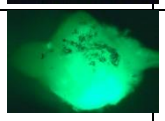	no	yes	no	no
266	UAS:GFP-HRAS^{V12} + UAS:Yap^{S5A}	40	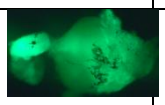	yes	no	yes	no
267	UAS:GFP-HRAS^{V12} + UAS:Yap^{S5A}	40	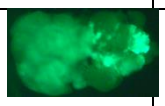	yes	yes	yes	no
268	UAS:Yap^{S5A}	47	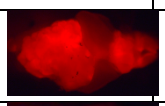	yes	no	yes	
269	UAS:Yap^{S5A}	54	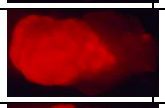	yes	yes	no	
270	UAS:Yap^{S5A}	54	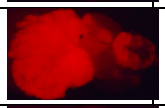	yes	yes	no	
271	UAS:Yap^{S5A}	54	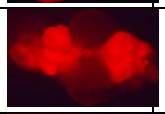	no	yes	no	
272	UAS:Yap^{S5A}	54	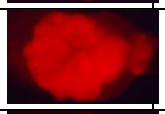	no	yes	no	
273	UAS:Yap^{S5A}	54	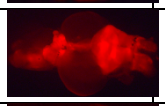	no	yes	no	
274	UAS:Yap^{S5A}	54	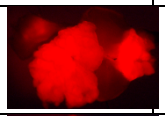	no	yes	no	
275	UAS:Yap^{S5A}	54	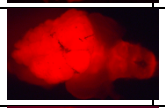	no	yes	no	
276	UAS:Yap^{S5A}	88	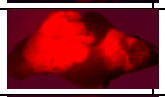	no	yes	yes	
277	UAS:Yap^{S5A}	88	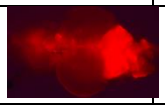	no	no	no	

278	UAS:Yap^{S5A}	88	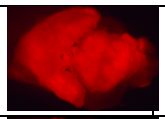	yes	yes	no
279	UAS:Yap^{S5A}	88	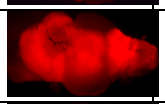	yes	yes	yes
280	UAS:Yap^{S5A}	88	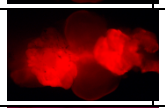	yes	no	yes
281	UAS:Yap^{S5A}	88	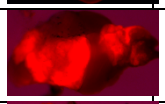	yes	yes	yes
282	UAS:Yap^{S5A}	76	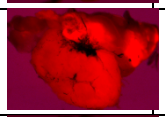	no	yes	no
283	UAS:Yap^{S5A}	76	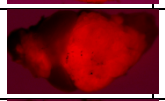	no	yes	yes
284	UAS:Yap^{S5A}	76	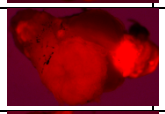	yes	yes	yes
285	UAS:Yap^{S5A}	76	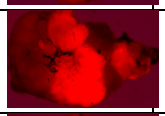	yes	yes	no
286	UAS:Yap^{S5A}	76	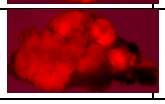	yes	yes	no

Table S3

Click here to Download Table S3

Table S4
List of YAP-related genes.

Ensemble Gene ID	log2(Fold Change)	adjusted pvalue	Gene Name
ENSDARG00000003293	1,571224817	2.42960518357847e-14	sox9a
ENSDARG00000005560	-0,510306743	0,007207761	ywhah
ENSDARG00000013078	-0,294928053	0,022141049	ywhaba
ENSDARG00000013207	0,574374872	0,002604248	zeb1b
ENSDARG00000016939	1,107244515	4.38714229014954e-06	itgb2
ENSDARG00000017953	1,070160674	0,078005579	tp73
ENSDARG00000023062	-0,626818162	0,137369882	cyr61
ENSDARG00000031246	0,870149527	0,045303211	hbegfb
ENSDARG00000031888	-0,448720304	0,008131336	mapk8a
ENSDARG00000034541	1,145555547	5.11709946291477e-10	tgfbr2
ENSDARG00000035873	2,029999584	8.72337651152246e-17	FJX1
ENSDARG00000040046	-0,587421331	0,318125688	snai2
ENSDARG00000041502	1,556557578	4.85106282821561e-05	tgfb1a
ENSDARG00000042518	0,174017463	0,342168185	hipk2
ENSDARG00000042934	1,684581537	4.4061432941375e-22	ctgfa
ENSDARG00000045482	-0,26735682	0,305865584	stk38l
ENSDARG00000046074	-0,245678658	0,424381998	stk11
ENSDARG00000052960	0,016107369	0,986059128	nppa
ENSDARG00000059483	0,713050005	0,01293987	tead1b
ENSDARG00000060010	0,834518645	0,002447814	iqgap2
ENSDARG00000063207	-0,877140352	7.92317473034202e-09	erbb4a
ENSDARG00000063309	-0,691094485	0,020763688	tjp2a
ENSDARG00000067626	-0,631573182	0,003117126	ywhag1
ENSDARG00000067719	0,769116894	0,004197799	wwtr1
ENSDARG00000068401	1,307768588	6.29935735788389e-06	yap1
ENSDARG00000070913	1,049586262	2.74457242921734e-09	sox2
ENSDARG00000075121	2,019581157	1.24955028420221e-19	hbegfa
ENSDARG00000075621	-0,784354196	0,195987459	birc5a
ENSDARG00000078335	1,431974201	1.2233826686997e-20	amot
ENSDARG00000078864	0,118871538	0,596309583	lats2
ENSDARG00000078888	1,949154437	1.89557208991909e-11	iqgap1
ENSDARG00000089536	-0,388858143	0,163063104	erbb4b
ENSDARG00000092260	-0,538246207	0,000125477	WBP1
ENSDARG00000026531	-0,246570951	0,215356428	alcama
ENSDARG00000058538	-0,557665776	NA	alcamb
ENSDARG00000061923	0,177676238	0,613424671	amotl2a
ENSDARG00000061948	0,439090942	0,430753957	amotl2b
ENSDARG00000063649	0,619532181	0,057323825	tead3b
ENSDARG00000074321	-0,121994384	0,874302367	tead3a

Table S5

Click here to Download Table S5

Table S6

Click here to Download Table S6